Unreliable homeostatic action potential broadening in cultured dissociated neurons

Andreas Ritzau-Jost[1,#], Salil Rajayer[2,3], Jana Nerlich[1], Filip Maciag[4], Alexandra John[1], Michael Russier[5], Victoria Gonzalez Sabater[6,7], Luke J. Steiger[2,3], Jacques-Olivier Coq[5], Jens Eilers[1], Maren Engelhardt[8,9,10], Juan Burrone[6,7], Dominique Debanne[5], Martin Heine[4], Stephen M Smith[2,3,#], Stefan Hallermann[1,#]

[1] Carl-Ludwig-Institute of Physiology, Faculty of Medicine, Leipzig University, Leipzig, 04103, Germany
[2] Division of Pulmonary and Critical Care Medicine, Department of Medicine, Oregon Health and Science University, Portland, Oregon, 97239-3098, USA
[3] Section of Pulmonary and Critical Care Medicine, VA Portland Health Care System, Portland, Oregon, 97239-2964, USA
[4] Institute for Developmental Biology and Neurobiology, Johannes Gutenberg University, Mainz, 55128, Germany
[5] Unité de Neurobiologie des canaux Ioniques et de la Synapse (UNIS), UMR_S 1072, INSERM, Aix-Marseille Université, Marseille, 13015, France
[6] MRC Centre for Neurodevelopmental Disorders, Institute of Psychiatry, Psychology and Neuroscience, King's College London, London, SE1 1UL, United Kingdom
[7] Centre for Developmental Neurobiology, Institute of Psychiatry, Psychology and Neuroscience, King's College London, London, SE1 1UL, United Kingdom
[8] Institute of Neuroanatomy, Mannheim Center for Translational Neuroscience, Medical Faculty Mannheim, Heidelberg University, Mannheim, 68167, Germany
[9] Institute of Anatomy and Cell Biology, Johannes Kepler University, Linz, 4020, Austria
[10] Clinical Research Institute for Neurosciences, Johannes Kepler University, Linz, 4020, Austria
[#] Correspondence: andreas.ritzau.jost@gmail.com (A.R-J.), smisteph@ohsu.edu (S.M.S.), and hallermann@medizin.uni-leipzig.de (S.H.)

Summary

Homeostatic plasticity preserves neuronal activity against perturbations. Recently, somatic action potential broadening was proposed as a key homeostatic adaptation to chronic inactivity in neocortical neurons. Since action potential shape critically controls calcium entry and neuronal function, broadening provides an attractive homeostatic feedback mechanism to regulate activity. Here, we report that chronic inactivity induced by sodium channel block does not broaden action potentials in neocortical neurons under a wide range of conditions. In contrast, action potentials were broadened in CA3 neurons of organotypic hippocampal cultures by chronic sodium channel block and in hippocampal dissociated cultures by chronic synaptic block. Mechanistically, BK-type potassium channels were proposed to underly inactivity-induced action potential broadening. However, BK channels did not affect action potential duration in our recordings. Our results indicate that action potential broadening can occur in specific neurons and conditions but is not a general mechanism of homeostatic plasticity in cultured neurons.

Introduction

Action potentials (APs) control various functions including neurotransmitter release from axonal boutons[1], calcium signals in the soma[2], and synaptic plasticity in dendrites[3]. AP broadening during short-term plasticity on the time scale of milliseconds to seconds is well-established and occurs in many types of neuronal cell bodies[4,5] and nerve terminals[6,7]. There are also indications that APs change during long-term plasticity on the time scale of minutes to hours. When examining Hebbian long-term plasticity (i.e., positive feedback-based and input-specific long-term plasticity[8]), some studies reported AP broadening. For example, presynaptic APs of hippocampal mossy fiber boutons broaden during depolarization-induced potentiation[9] and somatic APs of neurons in the amygdala broaden during fear conditioning[10]. In contrast, the role of the AP duration is less clear for non-Hebbian homeostatic long-term plasticity (i.e., negative feedback-based and non-input specific long-term plasticity[8]). Specifically, homeostatic plasticity induced by neuronal inactivity in the presence of the sodium channel blocker tetrodotoxin (TTX) has been studied for decades, but AP broadening was initially not described[11,12]. A recent study however reports prominent AP broadening during TTX-induced homeostatic plasticity at the soma of cultured neocortical neurons[13], which was not observed at presynaptic boutons of cultured neocortical neurons[14]. Compartmentalized AP broadening at the neuronal cell body would provide a strikingly simple and previously overlooked mechanism by which neuronal inactivity could increase subsequent excitability[13]. This mechanism involves decreased calcium entry during TTX application causing changes in gene expression that would result in broadened APs and more calcium entry after TTX removal. In this model, AP broadening is a key link in the homeostatic feedback loop underlying homeostatic plasticity. In a collaborative effort across several laboratories, we therefore systematically investigated AP broadening in cultured neurons during homeostatic plasticity under various experimental conditions.

Results

Cell type- and model-specific AP broadening in hippocampal neurons

APs in CA3 neurons of hippocampal organotypic slice cultures broaden homeostatically upon chronic inactivity using both, synaptic block by glutamate receptor antagonists[15] or sodium channel block by TTX[16] (see also ref. 17 for a similar trend). We first aimed to confirm homeostatic AP broadening in CA3 neurons in

organotypic slice cultures. APs were elicited by depolarizing currents from the resting membrane potential during perfusion with TTX-free artificial cerebrospinal fluid. APs recorded in CA3 pyramidal neurons treated with TTX (48 hours) had longer durations than those in control cells (Fig. 1A, B; median [IQR] 1.75 [1.69–1.86] ms and 2.13 [2.07–2.22] ms for control and TTX-treatment, respectively, 14 cells each, $P < 0.001$), confirming earlier reports of homeostatic AP broadening in these neurons[15,16].

Next, we tested whether homeostatic AP broadening occurred in dissociated hippocampal cultured neurons, a model widely used to study homeostatic plasticity. We inhibited neuronal activity for 48 hours to induce homeostatic plasticity by either blocking AP firing using TTX (Fig. 1C) or by blocking synaptic transmission using the low-affinity glutamate receptor blocker kynurenic acid (Kyn) or the high-affinity glutamate receptor blocker 2,3-Dioxo-6-nitro-1,2,3,4-tetrahydrobenzo [f]quinoxaline-7-sulfonamide (NBQX). Surprisingly, AP duration was unaffected by TTX-treatment in primary hippocampal cultured neurons (Fig. 1D; median [IQR] 2.07 [1.79–2.34] ms and 2.08 [1.32–2.61] ms for control and TTX, 25 and 24 cells, respectively, $P = 0.96$). In contrast, Kyn-treatment significantly increased AP duration in the same set of interleaved experiments (Fig. 1D; median [IQR] 2.52 [2.31–2.72] ms, 22 cells, $P = 0.014$) and NBQX-treatment led to a small trend towards broader APs (Fig. 1D; $P = 0.26$). Importantly, sodium channel block and synaptic block both increased spontaneous AP firing frequency, indicating that homeostatic adaptations other than AP broadening were shared between both induction methods (Fig. 1E, F; $P = 0.008$ for control against Kyn, $P = 0.005$ for control against NBQX, $P = 0.013$ for control against TTX). These data indicate that AP broadening occurred upon sodium channel block in CA3 neurons in organotypic slice cultures and upon synaptic block in dissociated hippocampal cultures, but not in the commonly-studied model of homeostatic plasticity using dissociated hippocampal cultured neurons and 48 hours of TTX application.

Stable AP duration in primary dissociated neurons during TTX-induced homeostatic plasticity

In contrast to our finding in dissociated cultured neurons of the hippocampus, a recent study described TTX-induced AP broadening in dissociated cultured neurons of the neocortex[13]. To resolve this discrepancy, we set out to replicate AP broadening in

114 neocortical cultured neurons. Given that exact reproduction of experimental conditions
115 is challenging and neuronal plasticity depends on brain region[18], animal species[19], and
116 animal strain[20], we probed homeostatic AP broadening under different experimental
117 conditions varying: 1) experimental animal species (rat and mouse), 2) strain (C57BL/6
118 and CD1 mice), 3) sub-strain (C57BL/6N and C57BL/6J mice), 4) brain area (cortex
119 and hippocampus), 5) cortical subdomain (prefrontal cortex), 6) culture duration (10–
120 14, 15–21, and 32 days *in vitro*), 7) culture growth medium, 8) recording solutions, and
121 9) laboratory and experimenter performing recordings (conditions I–X in Fig. 2B,
122 condition XI are recordings from Fig. 1; see also Fig. 2 – figure supplement 1). Even
123 though AP durations varied up to 2-fold between conditions, statistically significant
124 homeostatic AP broadening was not detectable in any of the tested conditions (Fig.
125 2B). To minimize type II errors (false negative) we intentionally did not apply a
126 correction for multiple comparisons. The only significance was observed in condition
127 III but in an opposite direction (i.e. AP narrowing with TTX, P=0.026; Fig. 2B). However,
128 this is likely a false positive because application of corrections for false discovery rate
129 results in P=0.268 for both Benjamini–Hochberg and Bonferroni correction. To detect
130 cross-conditional AP broadening by TTX, we merged all conditions based on their
131 difference in AP duration after TTX-treatment (Fig. 2C). However, AP duration was the
132 same in control and TTX-treated cells (217 and 197 cells, respectively, P = 0.83).
133
134 We next tested whether AP broadening was concealed by systematic differences in
135 neuronal health or recording quality between control and treatment group. Because
136 unhealthy neurons tend to have small and slow APs, possibly due to changes in resting
137 membrane potential or expression of voltage-gated sodium and potassium channels,
138 we first analyzed AP amplitude as a measure of neuronal viability. AP amplitudes were
139 not affected following TTX treatment in any of the eleven recording conditions (Fig. 2D)
140 or a cross-conditional comparison (Fig. 2E). In addition, we focused on the culture
141 protocol or cortical subdomain previously associated with AP broadening[13] (conditions
142 I, VII, and VIII) and applied further inclusion criteria to rigorously discriminate healthy
143 excitatory neurons: the occurrence of multiple APs upon 200 ms-current injections (≥
144 2 APs), a resting membrane potential below – 55 mV, and a maximum AP
145 depolarization rate between 100 and 337 V/s (includes 96% of excitatory and exclude
146 >80% of the inhibitory neurons; ref. 21). Applying any or all three of these criteria did
147 not reveal AP broadening upon TTX treatment (Fig. 2 – figure supplement 2). These

148 data indicate that stricter exclusion criteria result in smaller variability in action potential
149 duration but do not uncover AP broadening in these datasets.
150
151 Instead of depolarization-evoked APs, Li *et al.*[13] recorded hyperpolarization-evoked
152 'rebound APs' (Fig. 2F), possibly reducing the impact of different resting membrane
153 potentials and depolarizing current injection on the AP waveform. We determined that
154 the duration of rebound APs was similarly unaffected by TTX treatment across all
155 recorded conditions (Fig. 2G, H). These data show that TTX-induced AP broadening
156 does not robustly occur in dissociated cultured neurons.
157
158 **Homeostatic plasticity increases network activity and excitatory synaptic**
159 **transmission**
160 To verify successful induction of homeostatic plasticity under our experimental
161 conditions, we quantified changes in neuronal activity and synaptic strength following
162 TTX-induced homeostatic plasticity. TTX-treatment increased the number of
163 spontaneously active neurons (Fig. 3A; merge of conditions I–IV and VII; control: 23
164 out of 87 cells, TTX-treatment: 58 out of 74 cells, $P < 0.001$ with Fisher's exact test)
165 and the number of APs per spontaneous burst (Fig. 3B, C; median [IQR] 1.0 [1.0–1.12]
166 APs and 1.67 [1.0–2.71] APs for control and for TTX-treatment, 23 and 58 cells,
167 respectively, $P < 0.001$). These results indicate an adaptive increase in neuronal
168 activity following TTX-treatment, in line with previous findings on homeostatic
169 plasticity[16,22,23]. Furthermore, spontaneous excitatory postsynaptic currents (sEPSCs;
170 spontaneous synaptic currents recorded in the absence of TTX) were recorded as a
171 measure of synaptic strength (Fig. 3D). sEPSC frequency and amplitude increased
172 upon TTX-treatment (Fig. 2E, merge of recordings from condition I and II; median [IQR]
173 frequency 1.11 [0.42–1.47] Hz and 5.07 [1.95–5.52] Hz in control and TTX-treated
174 cells, 16 and 11, respectively, $P = 0.027$; median [IQR] amplitude 12.4 [10.6–14.4] pA
175 and 15.5 [14.1–17.4] pA in control and TTX-treated cells, 16 and 11 cells, respectively,
176 $P = 0.042$), in accord with known homeostatic synaptic adaptations to inactivity[24–27].
177 These changes in sEPSC amplitude and frequency are not specific for somatic, pre-
178 or postsynaptic adaptations. However, the results show that blocking AP firing with
179 TTX successfully induced homeostatic plasticity under our experimental conditions.
180

181 **Lack of BK channel-dependent AP broadening in dissociated cultured neurons**
182 Various potassium channel subtypes regulate AP repolarization and could therefore
183 underlie AP broadening. Li *et al.*[13] reported that downregulation of BK-type potassium
184 channels led to homeostatic AP broadening in neocortical cultured neurons. We tested
185 the role of BK channels in AP repolarization (neurons grown under condition I).
186 However, blocking BK channels with Iberiotoxin (IbTx, 300 nM) did not lead to
187 broadening of depolarization-evoked APs in control and TTX-treated cells (Fig. 4A; P
188 = 0.10 and 0.48, respectively), or a merge of both conditions (Fig. 4B; P = 0.10).
189 Rebound APs were similarly unaffected by BK channel block (Fig. 4 – figure
190 supplement 1). Next, we tested whether recurrent neuronal activity, which increases
191 cytosolic calcium and boosts BK-channel activity, enhanced AP broadening following
192 TTX treatment. While APs significantly broadened during repetitive firing, AP durations
193 were similar in control and TTX-treated neurons (Fig. 4C and D), suggesting no
194 differential regulation of BK-channels following TTX-treatment in these recordings.
195
196 In electrical recordings, intracellular recording solution may have disturbed cytosolic
197 calcium dynamics and therefore BK- and thus calcium-dependent AP repolarization.
198 As an independent approach, we recorded the AP duration in hippocampal cultured
199 neurons using the genetically encoded voltage indicator (GEVI) Ace-mNeon[28] before
200 and after acute IbTx perfusion (100 nM). BK channel block did not affect AP duration
201 in the soma or along the axon (Fig. 4E). Using the GEVI, we again tested the role of
202 BK channels in AP broadening during a train of APs (5 APs at 20 Hz, Fig. 4F). The
203 broadening of somatic, proximal axonal, and distal axonal APs during trains was similar
204 before and after BK channel block, indicating that AP duration was not modulated by
205 BK channels. To confirm that IbTx was indeed pharmacologically active in Ace-mNeon
206 recordings, we preconditioned cells with 4-AP (30 μM) prior to IbTx perfusion (Fig. 4G).
207 Neurons preconditioned with 4-AP had broader somatic APs which were further
208 broadened by IbTx, presumably due to increased calcium influx following 4-AP
209 treatment, in turn activating more BK channels[29]. These data indicate that IbTx
210 application was pharmacologically active but BK channels did not contribute to AP
211 repolarization in cultured neocortical neurons.
212

Discussion

Homeostatic AP broadening has been reported in some systems, but it has not been tested systematically across experimental models so far. Because BK channels that were proposed to underlie AP broadening are activated by depolarization and calcium[30,32], we studied APs elicited with depolarizations from the RMP where BK activity was presumably increased, as well as anode break ('rebound') APs thought to obviate variance from ion channel inactivation. We found that broadening of rebound and depolarization-evoked APs did not occur following the induction of homeostatic plasticity with TTX in the most commonly studied model system (primary dissociated neuronal cultures). However, AP broadening was observed in cultured hippocampal slices. Furthermore, blocking BK channels, which were reported to mediate AP broadening during homeostatic plasticity[13], did not impact AP duration in dissociated cultured neurons. Our results therefore indicate that AP broadening in cultured dissociated neurons is not a required component of homeostatic plasticity.

TTX-induced homeostatic AP regulation in organotypic hippocampal cultured neurons

AP broadening was previously shown to occur in CA3 neurons of organotypic hippocampal slice cultures following TTX-induced homeostatic plasticity[16]. Consistently, we recorded broader APs in CA3 neurons following neuronal inactivity (Fig. 1). In contrast to CA3 neurons, granule cells of the dentate gyrus did not show TTX-induced AP broadening[17]. Similarly, CA1 neurons did not show AP broadening following synaptic block-induced homeostatic plasticity[31]. Therefore, we conclude that homeostatic AP broadening in organotypic hippocampal cultures is most likely cell type-specific.

TTX-induced homeostatic AP regulation in primary dissociated cultured neurons

To the best of our knowledge, only three studies so far reported on the duration of APs following TTX-induced homeostatic plasticity in dissociated cultured neurons[13,33,34]. While Li *et al.*[13] observed TTX-induced broadening, the studies by Lee, Chung, and others[33,34] reported stable AP duration, consistent with our findings (Fig. 2). Furthermore, in other studies investigating TTX-induced homeostatic plasticity in dissociated cultured neurons, prominent AP broadening was either missed or absent (see for example refs. 23,35–37). One possible explanation for this inconsistency could

247 be the cell type-specificity of AP broadening. We focused on large, presumably
248 excitatory neurons. However, we and others could have selected different neuron
249 types compared to Li *et al.*[13]. In an attempt to reduce bias, we incorporated multi-lab,
250 randomization, and blinding strategies across many of our experiments. Only
251 recordings with leaky seal formation or inadequate capacitance compensation[38] were
252 excluded. However, in a subset of experimental conditions we applied additional
253 exclusion criteria to ensure that variability in neuron type, health or recording quality
254 were not causing a type II (false negative) statistical error. Application of these
255 exclusion criteria did not reveal AP broadening in our data (Fig. 2 – figure supplement
256 2), confirming that AP broadening was not associated with homeostatic plasticity in
257 neocortical neurons following TTX treatment.
258
259 The sensitivity to chronic TTX treatment might depend on baseline neuronal activity,
260 which is in part related to neuronal culture density[39]. However, TTX did not induce AP
261 broadening despite different baseline activities (Fig. 3A) and a nearly threefold
262 variation in the number of plated cells per cover slip between conditions (25k – 70k
263 cells per cover slip). Although we mainly focus on neocortical cultured neurons
264 (condition I to VIII, Fig. 2) because Li *et al.* used neocortical neurons, the absence of
265 AP broadening in hippocampal neurons (group IX to XI) could in principle be explained
266 by the selective loss of CA3 neurons, which show AP broadening in organotypic
267 cultured neurons (Fig. 1A and B). However, CA3 neurons were shown to survive in
268 dissociated cultures following region-specific microdissection[40], and CA1 neurons are
269 generally more stress-sensitive to excitotoxicity with glutamate or NMDA than CA3 and
270 DG neurons[42], arguing against a general selective loss of CA3 neuron in dissociated
271 cultures. Altered cell-cell interactions with glia and neurons in organotypic and
272 dissociated neuronal cultures could instead contribute to the different findings in
273 various hippocampal preparations.
274
275 **Synaptic block-induced homeostatic AP regulation in primary dissociated**
276 **cultured neurons**
277 Homeostatic AP broadening was shown in CA3 neurons upon activity block by the low-
278 affinity glutamate receptor blocker Kyn[15]. We similarly observed Kyn-induced AP
279 broadening in dissociated cultured hippocampal neurons (Fig. 1C, D). In contrast, APs
280 were not significantly broader following synaptic block by NBQX (Fig. 1C, D), in accord

281 with recordings from CA1 neurons in organotypic cultures using CNQX. TTX-induced
282 broadening may therefore be cell-type specific or due to a differential effect of the
283 glutamate receptor blockers on NMDA receptors which are blocked by Kyn but not
284 NBQX/CNQX or TTX and which have recently been demonstrated to be important for
285 the induction of synaptic homeostatic plasticity[41]. Further studies are needed to
286 investigate the role of subcellular calcium signals in the regulation of AP duration in
287 hippocampal neurons during block of glutamate receptors.
288
289 **Absence of BK channel-dependent AP broadening in dissociated cultured**
290 **neurons**
291 Li *et al.*[13] proposed that BK channels hasten AP repolarization and that this effect is
292 lost during TTX-induced homeostatic plasticity, leading to AP broadening. We did not
293 detect AP broadening when blocking BK channels in either control or TTX-treated cells
294 (Fig. 4). Furthermore, because calcium accumulation following multiple APs has been
295 shown to enhance intraspike BK contribution in some neurons[43] we compared how 1st,
296 2nd, or 3rd APs were impacted by prior TTX-exposure. AP broadening did occur in the
297 later APs but the changes were unaffected by TTX exposure (Fig. 4D), suggesting no
298 activity-dependent effect of TTX or BK channels on AP duration.
299
300 Voltage imaging using Ace-mNeon similarly showed that duration of single APs and
301 broadening during AP trains in the soma and axon were unaffected by BK channel
302 block. Blocking BK channels only affected AP repolarization when cells were
303 preconditioned with 4-AP. These results are consistent with previous reports showing
304 that in some neurons BK channels do not contribute to repolarization[43,44] while doing
305 so in others[44–47]. Differences in the abundance of other types of potassium channels[44]
306 and intracellular calcium buffering[46] are known to affect the contribution of BK channels
307 to AP repolarization and may account for the lack of AP broadening upon BK channel
308 block in our dissociated cultured neurons. Alternatively, BK activity may occur only
309 under conditions associated with elevated intracellular[30,32]. The lack of BK channel
310 contribution to AP repolarization in our dissociated neurons is another possible
311 explanation (in addition to different selection of cells) for why we and others have not
312 observed the homeostatic AP broadening described by Li *et al.*[13].
313
314 **Inactivity-induced homeostatic AP regulation *in vivo***

315 Homeostatic plasticity has also been studied using *in vivo* recordings from the activity-
316 suppressed visual cortex[48,49]. The majority of these studies reported stable AP duration
317 upon monocular deprivation or chemogenetic activity suppression[50–52]. In contrast, Li
318 *et al.*[13] found homeostatically broadened APs in the visual cortex upon monocular
319 deprivation. Furthermore, stable AP duration was also observed in other brain areas
320 following activity suppression such as (1.) the somatosensory cortex upon unilateral
321 whisker trimming[53–58] or forepaw denervation[59], (2.) the auditory system upon cochlear
322 ablation[60,61], hearing loss[62], or congenital deafness[63], (3.) the vestibular nucleus upon
323 vestibular ablation[64], and (4.) the olfactory mitral cells upon naris occlusion[65] or
324 senescent hippocampal deafferentiation[66]. Besides somatic APs, APs in excitatory
325 presynaptic terminals of the somatosensory thalamus were also unaffected by whisker
326 deprivation[67]. Thus, AP broadening does not appear to occur robustly upon
327 suppression of neuronal activity in various neuronal pathways.
328
329 **Hyperactivity-induced homeostatic AP regulation**
330 Homeostatic plasticity occurs not only upon activity block but also upon hyperactivity,
331 generally involving opposite adaptations. In cultured neurons, AP duration was
332 unaffected following hyperactivity induced by chronic depolarization[68], block of
333 potassium channels[69], block of inhibitory synaptic transmission[31,33,34], or chronic ChR2-
334 induced photostimulation[70]. In contrast, Li *et al.*[13] reported similar BK channel
335 downregulation upon both, TTX-induced activity block and depolarization-induced
336 hyperactivity.
337
338 As in cultured neurons, AP duration was mostly unaffected in brain slice recordings
339 from animals with increased neuronal activity due to an enriched environment[58,71,72],
340 psychosocial stress[73], or febrile seizures[74]. AP shortening occurred in cerebellar
341 granule cells after exposure to an enriched environment[75], in auditory neurons
342 following chronic noise exposure[76], and in hippocampal neurons following age-
343 related[77] or pilocarpine-induced hyperactivity[78]. Thus, in contrast to Li *et al.*[13], AP
344 duration was either unaffected or, if anything, shortened during hyperactivity-induced
345 homeostatic plasticity in previous studies.
346
347 In this study, several laboratories collaborated to determine the robustness of
348 inactivity-induced AP broadening. AP broadening did not occur upon TTX-treatment in

349 dissociated hippocampal or neocortical neurons. Furthermore, BK channel block did
350 not affect AP duration in dissociated neurons, arguing against BK channels as
351 mediators of a general homeostatic AP regulation.
352
353 Despite the lack of homeostatic, TTX-induced AP broadening in dissociated cultures,
354 AP duration was broadened upon Kyn-treatment in dissociated cultures and using TTX
355 in CA3 neurons in organotypic cultures. Because BK-channels control AP duration in
356 CA3 neurons of organotypic cultures[79], homeostatic BK-channel downregulation as
357 proposed by Li *et al.* may be involved in AP broadening in this specific cell type. While
358 the reasons for the variable occurrence of homeostatic AP broadening remain
359 unknown, this may render neuronal circuitries more robust to perturbations. The
360 regulation of AP duration therefore might represent one element in the repertoire of
361 neuronal plasticity that is, similar to other plasticity mechanisms, not generally shared,
362 but specifically expressed in some cell types and neuronal compartments.
363
364
365 **METHODS**
366 **Ethics**
367 At all times animal procedures were in accordance with the relevant international,
368 national and institutional guidelines for the care and use of laboratory animals
369 (European Council Directive 86/609/EEC, U.S. Public Health Service Policy on
370 Humane Care and Use of Laboratory Animals, U.S. National Institutes of Health Guide
371 for the Care and Use of Laboratory Animals, German Tierschutzgesetz, French
372 National Research Council guidelines, and Leipzig and Mainz University guidelines).
373 All animal procedures were approved in advance by the local health authorities (Ethics
374 Committees at Leipzig University and Mainz University, federal Saxonian Animal
375 Welfare Committee, the District administration Mainz-Bingen (41a/177-5865-§11
376 ZVTE), the Committee of the Préfecture des Bouches-du-Rhône (D13055-08), V.A.
377 Portland Health Care System Institutional Animal Care and Use Committee).
378
379 **Animal models**
380 Organotypic hippocampal cultures were generated from postnatal day 5–7 Wistar rats.
381 Dissociated neocortical cultures were generated from postnatal day 0 or 1 Sprague-
382 Dawley rats (conditions I, II and VII), C57BL/6N mice (conditions III and IV), C57BL/6J

383 mice (conditions V and VIII), or CD1 mice (condition VI). Dissociated hippocampal
384 cultures were generated from postnatal day 0 or 1 C57BL/6N mice (conditions IX),
385 C57BL/6J mice (condition X), or Sprague-Dawley rats (condition XI). Generally,
386 animals of both sexes were used to generate cultures. Mother animals were kept in
387 individually ventilated cages under a 12h/12h light-dark cycle and received water and
388 food *ad libitum*.
389
390 **Induction of Homeostatic Plasticity**
391 Homeostatic plasticity was induced by inclusion of one of the respective blockers in
392 culture medium for 48–56 hours prior to recordings. All blockers were first diluted in
393 100 µL of fresh medium per treated well and subsequently added to the respective
394 wells containing 1 mL of medium. For control conditions, only 100 µL of fresh medium
395 without blockers was added to the respective wells. The blockers had final
396 concentrations of (in mM): 0.002 tetrodotoxin (TTX; Tocris, Wiesbaden-Nordenstadt,
397 Germany), 2 kynurenic acid (Kyn), or 0.01 2,3-Dioxo-6-nitro-1,2,3,4-tetrahydrobenzo-
398 [f]quinoxaline-7-sulfonamide (NBQX). To avoid bias, coverslips were randomized to
399 treatment (control or blocker) and recordings were made and analyzed in a blinded
400 fashion (except for condition IV and VI). Blinding was performed by an independent
401 investigator. Control or TTX-treatment groups were assigned using an 8-block
402 randomization approach for experiments of condition VIII. Unblinding of the
403 experimental groups was performed after analysis and disclosure of the data by the
404 experimenter.
405
406 **Preparation of dissociated neocortical cultures**
407 *Conditions I and II (Hallermann Lab, Leipzig, Germany)*
408 Neocortical cultures were generated as described by Li *et al.*[13]. Shortly, neocortices
409 were isolated and dissected into 5–10 pieces per hemisphere. Samples were washed
410 twice in ice-cold modified HBSS (4.2 mM $NaHCO_3$ and 1 mM HEPES, pH 7.35, 300
411 mOsm) supplemented with 20% fetal bovine serum (FBS) and digested at 37 °C for 30
412 min using papain. After stopping digestion with 20% FBS-containing modified HBSS,
413 samples were washed and dissociated using Pasteur pipettes, pelleted twice, and
414 filtered using a 70 nm nylon strainer. 30.000–50.000 vital dissociated cells were plated
415 on poly-D-lysine-coated 14 mm coverslips and cultured in NbActive4 medium

416 (Transnetyx, Cordova, TN, USA) in an incubator until use (37 °C, 5% CO_2 in room air,
417 water vapor saturated).
418
419 *Conditions III and VII (Hallermann Lab, Leipzig, Germany)*
420 Cultures were generated as previously described by Moutin *et al.*[80]. In brief, mice were
421 decapitated and neocortices (for condition III) or the frontal third of neocortices (for
422 condition VII) were isolated in ice-cold Hibernate-A medium (Thermo Fisher Scientific,
423 Waltham, MA, USA) and cut into 5–10 chunks. Chunks were first digested by papain
424 (dissolved in Hibernate-A; 10 min at 37 °C) and subsequently by papain + DNAse (125
425 µL of 20 mg/mL DNAse stock; 5 min at 37 °C). Digestion was stopped by CM+ medium
426 (Neurobasal A 86.5 %, B27 2 %, Glutamax 0.25 %, L-Glutamine 0.25%, penicillin
427 G/streptomycin 1 %, heat-inactivated FBS 10 %) and chunks were mechanically
428 dissociated in two steps by 1250 µL pipette tips with gravity decantation and collection
429 of the supernatant between dissociation steps and after dissociation. Supernatant was
430 passed through 2 mL of frothed bovine serum albumin, centrifuged (7 min, 300 x g),
431 the resulting pellet was resuspended in 1–2 mL of CM+ medium and 25.000–30.000
432 resuspended vital cells were plated onto poly-L-lysine-coated coverslips. After 30 min,
433 0.5 mL of CM+ medium was added to the wells and after 2 days *in vitro* (DIV), cytosine
434 arabinoside (ARA-C, 1 µM final concentration) was added to the wells for 8–18 h.
435 Subsequently, 0.4 mL medium per well was replaced by fresh CM- medium (BrainPhys
436 96.75% by Stemcell Technologies, Vancouver, Canada, B27 2%, Glutamax 0.25%,
437 penicillin G/streptomycin 1%) and further 0.1 mL of medium were exchanged every 6–
438 7 days with fresh CM- medium until cells were used.
439
440 *Condition IV (Hallermann Lab, Leipzig, Germany)*
441 Cultures were generated following the protocol by Ritzau-Jost *et al.*[14]. In short, mice
442 were decapitated and cerebral cortices were removed, dissected in ice-cold Hank's
443 balanced saline solution, and cut into 5–10 pieces per hemisphere. Samples were
444 digested by Trypsin (5 mg, dissolved in digestion solution; for composition see below)
445 for 5 minutes at 37 °C. Trypsin was stopped by ice-cold MEM growth medium
446 (composition see below), supernatant was discarded, and samples were mechanically
447 and enzymatically dissociated using Pasteur pipettes of narrowing tip diameters in
448 DNAse-supplemented MEM growth medium (10 mg/mL). The supernatant was
449 centrifuged and the resulting pellet was resuspended in MEM growth medium for

450 plating onto Matrigel-coated 14 mm coverslips (50.000 vital cells/coverslip). Forty-eight
451 hours after plating, the medium was fully replaced by MEM growth medium containing
452 4 µM ARA-C to limit glial growth. After another 48 hours, the medium was fully replaced
453 by MEM growth medium. Cells were incubated at 37 °C, 93% humidity, and room air
454 plus 5% CO_2 until use. Digestion solution contained the following (in mM): 137 NaCl,
455 5 KCl, 7 Na_2HPO_4, 25 HEPES, pH adjusted to 7.2 by NaOH. MEM growth medium was
456 prepared from 1l MEM (Earle's salts + L-Glutamine) supplemented with 5 g Glucose,
457 0.2 g $NaHCO_3$, 0.1 g bovine holo-Transferrin, 0.025 g bovine insulin, 50 mL FBS and
458 10 mL B-27.
459
460 *Conditions V, VI and VIII (Smith Lab, Portland, OR, USA)*
461 Cultures were generated following the protocol by Martiszus *et al.*[81]. Briefly, 1–2-day
462 old mice were decapitated following general anesthesia with isoflurane, and their
463 cerebral cortices (for conditions V and VI) or the frontal third of neocortices (for
464 condition VIII) were dissected out while bathed in ice-cold modified Hank's balanced
465 saline solution (modified HBSS; Hyclone laboratories, Logan, UT, USA) and cut into
466 5–10 pieces per hemisphere. Samples were digested by Trypsin (10 mg, dissolved in
467 digestion solution as mentioned in Condition IV) for 5 minutes at 37 °C. Trypsin was
468 de-activated by ice-cold HBSS with 20% FBS, supernatant was discarded, and
469 samples were enzymatically and mechanically dissociated using Pasteur pipettes with
470 narrowing tip diameters in DNAse-supplemented HBSS. The supernatant was
471 centrifuged and the resulting pellet was resuspended in 5% MEM growth medium (see
472 composition above in Condition IV) for plating 65.000 vital cells onto Matrigel-coated
473 12 mm glass coverslips. MEM growth medium containing 4 µM ARA-C was added 48
474 hours later to limit glial proliferation, and subsequently replaced with MEM growth
475 medium following another 48 hours. Cells were incubated at 37 °C, 93% humidity, and
476 room air plus 5% CO_2 until use between days 11–14 *in vitro.*
477
478 **Preparation of dissociated hippocampal cultures**
479 *Condition IX and X (Heine Lab, Mainz, Germany)*
480 In short, mice pups were decapitated and brains were removed. Hippocampi were
481 dissected in ice-cold Hank's balanced saline solution and digested by trypsin for 15
482 minutes at 37 °C. Next, the tissue was washed with cold HBSS and mechanically
483 dissociated using Pasteur pipettes in DNAse-, glutamate- and FBS-supplemented

484 DMEM growth medium. 100 µL of cell suspension containing approximately 70.000
485 cells was placed on a glass coverslip and incubated at 37 °C, 5% CO_2 for 1 hour.
486 Coverslips were then transferred to 12-well plates with glutamate-, B27- and sodium
487 pyruvate-supplemented Neurobasal A medium (1 mL per well) and cultivated until use.
488 Double distilled water was added in between the wells of the 12-well plate to prevent
489 evaporation of the medium during cultivation.
490
491 *Condition XI (Hallermann Lab, Leipzig, Germany)*
492 Cultures were generated as described for Condition III, except that hippocampi from
493 postnatal day 0–1 Sprague-Dawley rats were used for preparation. 25.000–30.000 vital
494 cells were plated per coverslip.
495
496 **Recordings from dissociated cultures**
497 Within conditions, recordings were performed blinded (except conditions IV and VI)
498 and interleaved from randomized sister coverslips of the same culture, at the same
499 recording setup, and by the same experimenter.
500
501 *Conditions I – IV, VII and XI (Hallermann Lab, Leipzig, Germany)*
502 Voltage- and current-clamp recordings were performed with borosilicate pipettes using
503 a HEKA EPC10/2 amplifier (HEKA Elektronik, Lambrecht/Pfalz, Germany).
504 Borosilicate glass tubes (Science Products, Hofheim, Germany) were pulled by a DMZ
505 Universal Electrode Puller with filament heating (Zeitz Instruments, Martinsried,
506 Germany) to 3–6.5 MΩ pipette resistance. Pipettes were filled with internal solution
507 (see *Solutions and reagents* section) and mounted on a micromanipulator (Kleindiek
508 Nanotechnik, Reutlingen, Germany) using a custom-built pipette holder. Recordings
509 were performed at room temperature (22–25 °C). All current-clamp recordings were
510 filtered with the internal 10 kHz 8-pole Bessel filter of the HEKA EPC10/2 amplifier and
511 subsequently digitized (200 kHz) with the HEKA EPC10/2 using Patchmaster software
512 (HEKA Elektronik, Lambrecht/Pfalz, Germany). Built-in compensation was used for
513 voltage offset and pipette capacitance. Membrane potentials were not corrected for
514 liquid junction potential and bridge compensation was adjusted to minimize the current
515 injection artifact. APs were evoked by brief 1 ms depolarizing current injections of 500–
516 1500 pA or 500 ms hyperpolarizing pulses (300–1000 pA) leading to APs upon return
517 to resting membrane potential (‘rebound APs’). Both, depolarization-evoked and

518 rebound APs were first recorded at resting membrane potential without holding current.
519 While depolarization readily evoked APs in all conditions, rebound AP did not occur in
520 all conditions at their resting membrane potential. In these cells, holding currents were
521 used to depolarize cells until rebound APs were observed upon long hyperpolarizing
522 pulses. Spontaneous excitatory postsynaptic currents were recorded in voltage-clamp
523 mode at -70 mV membrane potential in neurons grown in conditions I and II. Currents
524 were filtered with the internal 3 kHz 8-pole Bessel filter of the HEKA EPC10/2 amplifier,
525 digitized (200 kHz) and detected using the template matching algorithm [82] implemented
526 in NeuroMatic (Version 2.00, 15.09.2008; ref. [83]).
527
528 *Conditions V, VI and VIII (Smith Lab, Portland, OR, USA)*
529 Current-clamp recordings were performed with borosilicate pipettes using a HEKA
530 EPC10 amplifier (HEKA Elektronik, Lambrecht/Pfalz, Germany). Patch pipettes (5–10
531 MΩ resistance) were pulled from thin-walled borosilicate glass tubes (Warner
532 Instruments, Holliston, MA, USA) using a P-87 electrode puller (Sutter Instruments,
533 Novato, CA, USA). Pipettes were filled with an internal solution (see *Solutions and*
534 *reagents* section) and mounted on a micromanipulator (ROE-200, Sutter Instruments,
535 Novato, CA, USA). Recordings were performed at room temperature (22–25 °C).
536 Voltage signals were filtered at 2.9 kHz and digitized at 20 kHz. Membrane potentials
537 were corrected for liquid junction potential and bridge balance was performed manually
538 prior to data acquisition. All APs were evoked by a sequence of transient injections
539 relative to the resting membrane potential and measurements taken from the APs
540 elicited with the minimal stimulus using either depolarizing current injections (500–
541 1000 pA in 100 pA increments for 1–3 ms in 0.5 ms increments in conditions V and VI
542 or 20–140 pA in 20 pA increments for 0.5 s in condition VIII) or following rebound from
543 longer hyperpolarizing pulses (300–1200 pA in 100 pA increments for 500 ms).
544
545 *Conditions IX & X (Heine Lab, Mainz, Germany)*
546 Voltage- and current-clamp recordings were performed with borosilicate pipettes using
547 a HEKA EPC9 amplifier (HEKA Elektronik, Lambrecht/Pfalz, Germany). Filamented
548 glass tubes (Science Products, Hofheim, Germany) were pulled by a Narishige PC-
549 100 electrode puller. Resistance of the pipettes was 2–6 MΩ. Pipettes were filled with
550 internal solution (see *Solutions and reagents* section) and mounted on a
551 micromanipulator (Luigs & Neumann, Ratingen, Germany). Recordings were

552 performed at room temperature (21–24 °C). Signals were filtered at 2.9 kHz and
553 digitized at 20 kHz using Patchmaster software (HEKA Elektronik, Lambrecht/Pfalz,
554 Germany). Built-in compensation was used for voltage offset and pipette capacitance.
555 Membrane potentials were not corrected for liquid junction potential. APs were evoked
556 by brief 1 ms depolarizing current injection of 50–300 pA or 500 ms hyperpolarizing
557 pulses (300–400 pA) leading to APs upon return to resting membrane potential
558 ('rebound APs').
559
560 **Preparation of organotypic hippocampal cultures**
561 Cultures were prepared as described previously[84]. In brief, young Wistar rats (P5–P7)
562 were anesthetized with isoflurane and killed by decapitation, the brain was removed,
563 and each hippocampus was dissected. Hippocampal slices (350 µm) were obtained
564 using a Vibratome (Leica, VT1200S, Wetzlar, Germany). They were placed on 20 mm
565 latex membranes (Millicell; Merck, Darmstadt, Germany) inserted into 35 mm Petri
566 dishes containing 1 mL of culture medium and maintained for up to 8 days in an
567 incubator at 34 °C, 95% O_2, 5% CO_2. The culture medium contained 25 mL MEM, 12.5
568 mL HBSS, 12.5 mL horse serum, 0.5 mL penicillin/streptomycin, 0.8 mL glucose (1 M),
569 0.1 mL ascorbic acid (1 mg/mL), 0.4 mL HEPES (1 M), 0.5 mL B27, and 8.95 mL sterile
570 H_2O. To limit glial proliferation, 5 µM ARA-C was added to the culture medium starting
571 at DIV 4.
572
573 **AP recordings from organotypic hippocampal cultures**
574 Whole-cell recordings were obtained from CA3 neurons in organotypic cultures at DIV
575 7 to DIV 10. All recordings were made at 34 °C in a temperature-controlled recording
576 chamber (Luigs & Neumann, Ratingen, Germany) using 7–10 MΩ patch pipettes. CA3
577 pyramidal neurons were recorded in current-clamp with a Multiclamp 700B Amplifier
578 (Molecular Devices, San Jose, CA, USA). APs were elicited by delivering DC step
579 pulses (duration 1.0 s) at an interstimulus interval of 10–15 s. During the whole
580 recording, ionotropic glutamate and $GABA_A$ receptors were blocked with 2–4 mM
581 kynurenic acid and 100 µM picrotoxin, respectively.
582
583 **Analysis of APs**
584 Data were analyzed using IGOR PRO software (WaveMetrics, Lake Oswego, OR,
585 USA; Version 6.32A or 6.37), the Patcher's Power Tool (Version 2.19 Carbon,

586 15.03.2011) and NeuroMatic (Version 2.00, 15.09.2008; ref. [83]) extensions, as well as
587 self-written IGOR PRO scripts. AP durations were quantified as the duration at half-
588 maximal AP amplitude, amplitude being the difference between AP peak and the
589 membrane potential preceding stimulation. When AP durations were recorded at half-
590 maximal amplitude between AP threshold (defined as the membrane potential at which
591 the voltage rate of change first reaches 10 V/s) and AP peak, AP durations were still
592 unaffected by TTX treatment (data not shown). To exclude the effect of mis-balanced
593 bridge compensation on AP shape, only APs that occurred after the end of the second
594 current injection artifact (elicited by the end of current-injection) were analyzed. In
595 some recordings, current injection artifacts were blanked over 50 µs at the beginning
596 and the end of the current injection and only experiments in which blanking did not
597 affect AP amplitude and duration were subsequently analyzed.
598
599 **Hippocampal dissociated cultures and transfection for GEVI imaging**
600 Culture preparation and GEVI transfection were performed as previously described by
601 Sabater *et al.*[28]. In short, hippocampi were dissected from embryonic day 17.5 Wistar
602 rat pups of either sex, treated with trypsin (Worthington Biochemical Corporation,
603 Lakewood, NJ, USA) at 0.5 mg/mL, and mechanically dissociated using fire polished
604 Pasteur pipettes. Neurons were plated on 18 mm glass coverslips pre-treated with 100
605 µg/mL poly-L-lysine and coated with 10 µg/mL laminin (Thermo Fisher Scientific,
606 Waltham, MA, USA). Cultures were maintained in Neurobasal medium with B27 (1x)
607 and GlutaMAX (1x, all obtained from Thermo Fisher Scientific, Waltham, MA, USA),
608 supplemented with FBS (2%, Biosera, Nuaille, France) and Penicillin/Streptomycin
609 (1%, Sigma-Aldrich, St. Louis, MO, USA), at 37°C in a humidified incubator with 5%
610 CO_2. For transfections with Ace2N-mNeon-4AA (Ace-mNeon, ref. [85]; distributed by
611 Biolife Solutions Inc., Bothell, WA, USA), the Effectene transfection reagent (Qiagen,
612 Venlo, Netherlands) was used. The medium was changed at DIV 3 to culture medium
613 without antibiotic or FBS, and transfections with Effectene were performed at DIV 7
614 following the manufacturer's protocol. After transfection neurons were maintained in
615 serum-free media without antibiotics. For all experiments 30% of the medium was
616 changed weekly and neurons were imaged 7–14 days after transfection (14–21 DIV).
617
618 **GEVI Imaging conditions**

619 GEVI imaging was performed as previously described by Sabater *et al.*[28]. In short,
620 neurons were imaged using an inverted Olympus IX71 epifluorescence microscope
621 with a 60x 1.42 NA oil-immersion objective (Olympus, Tokyo, Japan). Coverslips were
622 mounted in a heated chamber (Warner instruments, Holliston, MA, USA; total volume
623 ~500 µL) and placed on an IMTP microscope stage (Scientifica, Uckfield, United
624 Kingdom). Cells were maintained in external HEPES-buffered saline solution (HBS: 2
625 mM $CaCl_2$, 1.6 mM $MgCl_2$, 1.45 mM NaCl, 2.5 mM KCl, 10 mM Glucose, 10 mM
626 HEPES, pH 7.4, Osmolarity 290 mOsm) and experiments were carried out at near
627 physiological temperatures of 32–35 ºC.
628
629 In Ace-mNeon imaging experiments, ~505 nm excitation illumination was provided
630 using a 525 nm LED (Solis LED, Thorlabs, Newton, NJ, USA), a 500/20 nm excitation
631 filter, and a 510 nm long-pass dichroic mirror. Ace-mNeon emission transmitted
632 through the dichroic was filtered using a 520 nm long-pass filters (Chroma, Bellows
633 Falls, VT, USA). A power density of 10 mW/mm^2 was obtained at the specimen plane.
634 Images were acquired at 3.2 kHz with an ORCA-Flash4.0 V2 C11440-22CU scientific
635 CMOS camera (Hamamatsu Photonics, Hamamatsu, Japan) cooled to ~ -20 ºC with
636 the Exos2 water cooling system (Koolance, Auburn, WA, USA). Images were acquired
637 with HCImage software (Hamamatsu, Hamamatsu, Japan), binned to 4 × 4 and
638 cropped to a 16 × 512-pixel region of interest, necessary to achieve the high image
639 acquisition rates. Images were saved in CXD format.
640
641 Stimulation of APs was achieved with an extracellular tungsten parallel bipolar
642 electrode (FHC, Bowdoin, ME, USA) mounted on a PatchStar motorized micro-
643 manipulator (Scientifica, Uckfield, United Kingdom). To reliably induce an AP, we
644 delivered a 1 ms 10 mV pulse at the soma. The timing of the LED illumination, the
645 acquisition and stimulation were triggered externally through Clampex software
646 (pClamp 10, Molecular Devices, San Jose, CA, USA).
647
648 All GEVI Imaging recordings were performed in presence of NBQX (10 µM), Gabazine
649 (10 µM) and D-2-amino-5-phosphonovalerate (APV, 25 µM; all from Bio-Techne,
650 Wiesbaden-Nordenstadt, Germany) in order to block synaptic transmission and ensure
651 that the observed events were due to the stimulation only. IbTx was delivered using a

652 custom gravity-fed perfusion system and bath volume was maintained by a peristaltic
653 pump (Watson-Marlow 120s; Watson-Marlow, Rommerskirchen, Germany).
654
655 **Image analysis**
656 Image analysis was performed as previously described by Sabater *et al.*[28]. In short,
657 voltage imaging recordings were analyzed in ImageJ and custom scripts within
658 MATLAB software as follows. Prior to analysis, if drift had occurred in the x and y axis
659 during the recording, the images were aligned using the TurboReg ImageJ plugin[86].
660 Images were then imported into MATLAB and fluorescence intensity profiles were
661 obtained from regions of interest (ROIs) manually drawn around neuronal structures
662 identified visually on a maximum projection image of the time series by averaging
663 across the ROI pixels in each frame. The fluorescence profile was separated into single
664 trials and corrected for background camera noise by subtracting the average intensity
665 value of the timepoints where no illumination light was applied. Then, recordings were
666 reconstructed at a sampling rate of 100 kHz using cubic spline interpolation. Bleaching
667 was estimated by fitting a single exponential function to each individual trace smoothed
668 using an averaging filter with a window of 3 and interpolated. The resulting curve was
669 used to correct an unfiltered interpolated version of the recording. An accurate
670 representation of the AP waveform with an enhanced SNR was obtained by averaging
671 over the repeats and extracting the AP parameters from the resulting trace. The
672 fluorescence profile during the 20 ms preceding a response was used as baseline.
673
674 **Solutions and reagents**
675 Reagents were purchased from Sigma-Aldrich (St. Louis, MO, USA) if not indicated
676 otherwise.
677
678 *Conditions I, II, VII and XI*
679 The extracellular bath solution contained (in mM): 122 NaCl, 3 KCl, 10 D-Glucose, 26
680 $NaHCO_3$, 1.25 Na_2HPO_4, 1.3 $MgCl_2$, and 2.0 $CaCl_2$. After equilibration with 95% O_2–
681 5% CO_2, pH was adjusted to 7.35 if needed by NaOH or HCl. The intracellular pipette
682 solution contained (in mM): 130 K gluconate, 1 $MgCl_2$, 10 HEPES, 0.3 EGTA, 10 Tris-
683 Phosphocreatine, 4 Mg-ATP, 0.3 Na-GTP. When testing the contribution of BK
684 channels, 300 nM Iberiotoxin (Abcam, Cambridge, United Kingdom) was included in
685 the bath solution.

686

687 *Conditions III and IV*

688 The extracellular bath solution contained (in mM): 125 NaCl, 3 KCl, 25 Glucose, 25
689 $NaHCO_3$, 1.25 Na_2HPO_4, 1.1 $MgCl_2$, and 1.1 $CaCl_2$. After equilibration with 95% O_2–
690 5% CO_2, pH was adjusted to 7.35 if needed by NaOH or HCl. The intracellular pipette
691 solution contained (in mM): 150 K Gluconate, 10 K-HEPES, 3 Mg-ATP, 0.3 Na-GTP,
692 0.05 EGTA, 10 NaCl.

693

694 *Conditions V and VI*

695 The extracellular bath solution contained (in mM): 150 NaCl, 4 KCl, 10 HEPES, 10
696 glucose, 1.0 $MgCl_2$, and 2.0 $CaCl_2$, and was equilibrated with 95% O_2–5% CO_2. The
697 intracellular pipette solution contained (in mM): 135 K gluconate, 4 NaCl, 0.05 EGTA,
698 10 HEPES, 3 $MgCl_2$, 0.3 NaGTP, 3 Na_2ATP, 10 Na_2-Creatine phosphate with pH
699 normalized to 7.25 using KOH.

700

701 *Condition VIII*

702 The extracellular bath solution contained (in mM): 122 NaCl, 3 KCl, 1.25 NaH_2PO_4, 26
703 $NaHCO_3$, 10 glucose, 1.3 $MgCl_2$, and 2.0 $CaCl_2$, and was bubbled with 95% O_2–5%
704 CO_2. The intracellular pipette solution contained (in mM): 130 K gluconate, 0.3 EGTA,
705 10 HEPES, 2 $MgCl_2$, 0.3 NaGTP, 4 Na_2ATP (or Mg-ATP), 10 Na_2-Creatine phosphate
706 (or Tris-Creatinine phosphate).

707

708 *Conditions IX and X*

709 The extracellular bath solution contained (in mM): 145 NaCl, 2.5 KCl, 10 HEPES, 24
710 glucose, 1.3 $MgCl_2$, and 2.0 $CaCl_2$, and was equilibrated with 95% O_2–5% CO_2. The
711 intracellular pipette solution contained (in mM): 140 K gluconate, 2 NaCl, 0.5 EGTA,
712 20 HEPES, 3 $MgCl_2$, 0.3 NaGTP, 4 Na_2ATP, with pH adjusted to 7.25 using KOH.

713

714 *Organotypic hippocampal neuron recordings*

715 The external bath solution contained (in mM): 125 NaCl, 26 $NaHCO_3$, 3 $CaCl_2$, 2.5 KCl,
716 2 $MgCl_2$, 0.8 NaH_2PO_4, and 10 D-glucose, and was equilibrated with 95% O_2–5% CO_2.
717 The intracellular pipette solution contained (mM): 120 K gluconate, 20 KCl, 10 HEPES,
718 0.5 EGTA, 2 $MgCl_2$, 2 Na_2ATP, and 0.3 NaGTP (pH 7.4).

719

720 **Statistics**

721 If not otherwise noted, data are expressed as box plots with boxes reflecting 25th–75th
722 percentile. The median is indicated by a line within the box, whiskers indicate 10th and
723 90th percentile. Sample sizes (n) provide the number of individual somatic recordings.
724 All data sets were obtained from ≥ 2 independent cell cultures. Data in Fig. 3A were
725 tested for statistical difference using Fisher's exact test. Confidence limits for 95%
726 confidence intervals were calculated as Wilson interval[87]. Other experimental groups
727 were independent and tested by the Mann-Whitney *U* test. Tests were performed in
728 IGOR PRO or GraphPad Prism 8. Results were considered significant at $p < 0.05$.
729

730 **Acknowledgment**

731 This work was supported by a European Research Council Consolidator Grant (ERC
732 CoG 865634) the German Research Foundation (HA6386/10-2) to S.H. and by grants
733 awarded by the U.S. Department of Veterans Affairs (BX002547) and NIGMS
734 (GM134110) to S.M.S.
735

736 **Declaration of interests**

737 The authors declare no competing interests.
738

739 **References**

740 1. Borst, J.G.G., and Sakmann, B. (1999). Effect of changes in action potential
741 shape on calcium currents and transmitter release in a calyx-type synapse of
742 the rat auditory brainstem. Philosophical Transactions of the Royal Society B:
743 Biological Sciences *354*, 347–355. https://doi.org/10.1098/RSTB.1999.0386.
744 2. Christie, B.R., Eliot, L.S., Ito, K.I., Miyakawa, H., and Johnston, D. (1995).
745 Different Ca2+ channels in soma and dendrites of hippocampal pyramidal
746 neurons mediate spike-induced Ca2+ influx. J. Neurophysiol. *73*, 2553–2557.
747 https://doi.org/10.1152/jn.1995.73.6.2553.
748 3. Watanabe, S., Hoffman, D.A., Migliore, M., and Johnston, D. (2002). Dendritic
749 K+ channels contribute to spike-timing dependent long-term potentiation in
750 hippocampal pyramidal neurons. Proc. Natl. Acad. Sci. U. S. A. *99*, 8366–8371.
751 https://doi.org/10.1073/PNAS.122210599.
752 4. Bean, B.P. (2007). The action potential in mammalian central neurons. Nat.
753 Rev. Neurosci. *8*, 451–465. https://doi.org/10.1038/nrn2148.
754 5. Debanne, D., Campanac, E., Bialowas, A., Carlier, E., and Alcaraz, G. (2011).
755 Axon physiology. Physiol. Rev. *91*, 555–602.
756 https://doi.org/10.1152/PHYSREV.00048.2009.
757 6. Geiger, J.R.P., and Jonas, P. (2000). Dynamic control of presynaptic Ca2+
758 inflow by fast-inactivating K+ channels in hippocampal mossy fiber boutons.
759 Neuron *28*, 927–939. https://doi.org/10.1016/S0896-6273(00)00164-1.
760 7. Jackson, M.B., Konnerth, A., and Augustine, G.J. (1991). Action potential
761 broadening and frequency-dependent facilitation of calcium signals in pituitary
762 nerve terminals. Proc. Natl. Acad. Sci. U. S. A. *88*, 380–384.
763 https://doi.org/10.1073/PNAS.88.2.380.
764 8. Keck, T., Toyoizumi, T., Chen, L., Doiron, B., Feldman, D.E., Fox, K., Gerstner,
765 W., Haydon, P.G., Hübener, M., Lee, H.K., et al. (2017). Integrating Hebbian
766 and homeostatic plasticity: The current state of the field and future research
767 directions. Philosophical Transactions of the Royal Society B: Biological
768 Sciences *372*. https://doi.org/10.1098/rstb.2016.0158.
769 9. Carta, M., Lanore, F., Rebola, N., Szabo, Z., Da Silva, S.V., Lourenço, J.,
770 Verraes, A., Nadler, A., Schultz, C., Blanchet, C., et al. (2014). Membrane
771 lipids tune synaptic transmission by direct modulation of presynaptic potassium
772 channels. Neuron *81*, 787–799.
773 https://doi.org/10.1016/J.NEURON.2013.12.028.
774 10. Senn, V., Wolff, S.B.E., Herry, C., Grenier, F.O., Ehrlich, I., Grü, J., Fadok,
775 J.P., Müller, C., Letzkus, J.J., and Lüthi, A. (2014). Long-range connectivity
776 defines behavioral specificity of amygdala neurons. Neuron *81*, 428–437.
777 https://doi.org/10.1016/j.neuron.2013.11.006.
778 11. Turrigiano, G.G., and Nelson, S.B. (2004). Homeostatic plasticity in the
779 developing nervous system. Nat. Rev. Neurosci. *5*, 97–107.
780 https://doi.org/10.1038/nrn1327.
781 12. Pozo, K., and Goda, Y. (2010). Unraveling mechanisms of homeostatic
782 synaptic plasticity. Neuron *66*, 337–351.
783 https://doi.org/10.1016/J.NEURON.2010.04.028.
784 13. Li, B., Suutari, B.S., Sun, S.D., Luo, Z., Wei, C., Chenouard, N., Mandelberg,
785 N.J., Zhang, G., Wamsley, B., Tian, G., et al. (2020). Neuronal inactivity co-
786 opts LTP machinery to drive potassium channel splicing and homeostatic spike
787 widening. Cell *181*, 1547-1565.e15. https://doi.org/10.1016/j.cell.2020.05.013.
788 14. Ritzau-Jost, A., Tsintsadze, T., Krueger, M., Ader, J., Bechmann, I., Eilers, J.,
789 Barbour, B., Smith, S.M., and Hallermann, S. (2021). Large, stable spikes

exhibit differential broadening in excitatory and inhibitory neocortical boutons. Cell Rep. *34*, 108612. https://doi.org/10.1016/j.celrep.2020.108612.

15. Zbili, M., Rama, S., Benitez, M.J., Fronzaroli-Molinieres, L., Bialowas, A., Boumedine-Guignon, N., Garrido, J.J., and Debanne, D. (2021). Homeostatic regulation of axonal Kv1.1 channels accounts for both synaptic and intrinsic modifications in the hippocampal CA3 circuit. Proc. Natl. Acad. Sci. U. S. A. *118*. https://doi.org/10.1073/pnas.2110601118.
16. Kim, J., and Tsien, R.W. (2008). Synapse-specific adaptations to inactivity in hippocampal circuits achieve homeostatic gain control while dampening network reverberation. Neuron *58*, 925–937. https://doi.org/10.1016/j.neuron.2008.05.009.
17. Mitra, A., Mitra, S.S., and Tsien, R.W. (2012). Heterogeneous reallocation of presynaptic efficacy in recurrent excitatory circuits adapting to inactivity. Nat. Neurosci. *15*, 250–257. https://doi.org/10.1038/nn.3004.
18. Castro-Alamancos, M.A., and Connors, B.W. (1997). Distinct forms of short-term plasticity at excitatory synapses of hippocampus and neocortex. Proc. Natl. Acad. Sci. U. S. A. *94*, 4161–4166. https://doi.org/10.1073/pnas.94.8.4161.
19. Manahan-Vaughan, D. (2018). Special considerations when using mice for In vivo electrophysiology and long-term studies of hippocampal synaptic plasticity during behavior. Handb. Behav. Neurosci. *28*, 63–84. https://doi.org/10.1016/B978-0-12-812028-6.00003-3.
20. Nguyen, P. V., Duffy, S.N., and Young, J.Z. (2000). Differential maintenance and frequency-dependent tuning of LTP at hippocampal synapses of specific strains of inbred mice. J. Neurophysiol. *84*, 2484–2493. https://doi.org/10.1152/jn.2000.84.5.2484.
21. Prestigio, C., Ferrante, D., Valente, P., Casagrande, S., Albanesi, E., Yanagawa, Y., Benfenati, F., and Baldelli, P. (2019). Spike-Related Electrophysiological Identification of Cultured Hippocampal Excitatory and Inhibitory Neurons. Mol. Neurobiol. *56*, 6276–6292. https://doi.org/10.1007/s12035-019-1506-5.
22. Maffei, A., and Turrigiano, G.G. (2008). Multiple modes of network homeostasis in visual cortical layer 2/3. Journal of Neuroscience *28*, 4377–4384. https://doi.org/10.1523/JNEUROSCI.5298-07.2008.
23. Desai, N.S., Rutherford, L.C., and Turrigiano, G.G. (1999). Plasticity in the intrinsic excitability of cortical pyramidal neurons. Nat. Neurosci. *2*, 515–520. https://doi.org/10.1038/9165.
24. Turrigiano, G.G., Leslie, K.R., Desai, N.S., Rutherford, L.C., and Nelson, S.B. (1998). Activity-dependent scaling of quantal amplitude in neocortical neurons. Nature *391*, 892–896. https://doi.org/10.1038/36103.
25. Hanes, A.L., Koesters, A.G., Fong, M.-F., Altimimi, H.F., Stellwagen, D., Wenner, P., and Engisch, K.L. (2020). Cellular/molecular divergent synaptic scaling of miniature EPSCs following activity blockade in dissociated neuronal cultures. *40*, 4090–4102. https://doi.org/10.1523/JNEUROSCI.1393-19.2020.
26. Frank, C.A., Kennedy, M.J., Goold, C.P.P., Marek, K.W., and Davis, G.W.W. (2006). Mechanisms underlying the rapid induction and sustained expression of synaptic homeostasis. Neuron *52*, 663–677. https://doi.org/10.1016/J.NEURON.2006.09.029.
27. Aoto, J., Nam, C.I., Poon, M.M., Ting, P., and Chen, L. (2008). Synaptic Signaling by All-Trans Retinoic Acid in Homeostatic Synaptic Plasticity. Neuron *60*, 308–320. https://doi.org/10.1016/j.neuron.2008.08.012.

28. Gonzalez Sabater, V., Rigby, M., and Burrone, J. (2021). Voltage-gated potassium channels ensure action potential shape fidelity in distal axons. The Journal of Neuroscience *41*, 5372–5385. https://doi.org/10.1523/jneurosci.2765-20.2021.
29. Hu, H., Shao, L.-R., Chavoshy, S., Gu, N., Trieb, M., Behrens, R., Laake, P., Pongs, O., Knaus, H.G., Ottersen, O.P., et al. (2001). Presynaptic Ca2+-activated K+ channels in glutamatergic hippocampal terminals and their role in spike repolarization and regulation of transmitter release. The Journal of Neuroscience *21*, 9585–9597. https://doi.org/10.1523/JNEUROSCI.21-24-09585.2001.
30. Lorenzo-Ceballos, Y., Carrasquel-Ursulaez, W., Castillo, K., Alvarez, O., and Latorre, R. (2019). Calcium-driven regulation of voltagesensingdomains in BK channels. Elife *8*, 1–24. https://doi.org/10.7554/eLife.44934.
31. Karmarkar, U.R., and Buonomano, D. V. (2006). Different forms of homeostatic plasticity are engaged with distinct temporal profiles. European Journal of Neuroscience *23*, 1575–1584. https://doi.org/10.1111/j.1460-9568.2006.04692.x.
32. Horrigan, F.T., and Aldrich, R.W. (2002). Coupling between voltage sensor activation, Ca2+ binding and channel opening in large conductance (BK) potassium channels. Journal of General Physiology *120*, 267–305. https://doi.org/10.1085/jgp.20028605.
33. Lee, K.Y., and Chung, H.J. (2014). NMDA receptors and L-type voltage-gated Ca2+ channels mediate the expression of bidirectional homeostatic intrinsic plasticity in cultured hippocampal neurons. Neuroscience *277*, 610–623. https://doi.org/10.1016/j.neuroscience.2014.07.038.
34. Lee, K.Y., Royston, S.E., Vest, M.O., Ley, D.J., Lee, S., Bolton, E.C., and Chung, H.J. (2015). N-methyl-D-aspartate receptors mediate activity-dependent down-regulation of potassium channel genes during the expression of homeostatic intrinsic plasticity. Mol. Brain *8*, 1–16. https://doi.org/10.1186/s13041-015-0094-1.
35. Zhao, C.J., Dreosti, E., and Lagnado, L. (2011). Homeostatic synaptic plasticity through changes in presynaptic calcium influx. Journal of Neuroscience *31*, 7492–7496. https://doi.org/10.1523/JNEUROSCI.6636-10.2011.
36. Desai, N.S., Rutherford, L.C., and Turrigiano, G.G. (1999). BDNF regulates the intrinsic excitability of cortical neurons. Learning and Memory *6*, 284–291. https://doi.org/10.1101/lm.6.3.284.
37. Rutherford, L.C., DeWan, A., Lauer, H.M., and Turrigiano, G.G. (1997). Brain-derived neurotrophic factor mediates the activity-dependent regulation of inhibition in neocortical cultures. Journal of Neuroscience *17*, 4527–4535. https://doi.org/10.1523/jneurosci.17-12-04527.1997.
38. Ritzau-Jost, A., Nerlich, J., Kaas, T., Krueger, M., Tsintsadze, T., Eilers, J., Barbour, B., Smith, S.M., and Hallermann, S. (2023). Direct whole-cell patch-clamp recordings from small boutons in rodent primary neocortical neuron cultures. STAR Protoc. *4*, 102168. https://doi.org/10.1016/j.xpro.2023.102168.
39. Ivenshitz, M., and Segal, M. (2010). Neuronal density determines network connectivity and spontaneous activity in cultured hippocampus. J. Neurophysiol. *104*, 1052–1060. https://doi.org/10.1152/jn.00914.2009.
40. Mattson, M.P., and Kater, S.B. (1989). Development and selective neurodegeneration in cell cultures from different hippocampal regions. Brain Res. *490*, 110–125. https://doi.org/https://doi.org/10.1016/0006-8993(89)90436-8.

41. Chipman, P.H., Fetter, R.D., Panzera, L.C., Bergerson, S.J., Karmelic, D., Yokoyama, S., Hoppa, M.B., and Davis, G.W. (2022). NMDAR-dependent presynaptic homeostasis in adult hippocampus: Synapse growth and cross-modal inhibitory plasticity. Neuron *110*, ki. https://doi.org/10.1016/j.neuron.2022.08.014.
42. Vinet, J., van Weering, H.R.J., Heinrich, A., Kälin, R.E., Wegner, A., Brouwer, N., Heppner, F.L., van Rooijen, N., Boddeke, H.W.G.M., and Biber, K. (2012). Neuroprotective function for ramified microglia in hippocampal excitotoxicity. J. Neuroinflammation *9*, 1–15. https://doi.org/10.1186/1742-2094-9-27.
43. Niday, Z., and Bean, B.P. (2021). BK channel regulation of afterpotentials and burst firing in cerebellar purkinje neurons. Journal of Neuroscience *41*, 2854–2869. https://doi.org/10.1523/JNEUROSCI.0192-20.2021.
44. Gittis, A.H., Moghadam, S.H., and Du Lac, S. (2010). Mechanisms of sustained high firing rates in two classes of vestibular nucleus neurons: Differential contributions of resurgent Na, Kv3, and BK currents. J. Neurophysiol. *104*, 1625–1634. https://doi.org/10.1152/jn.00378.2010.
45. Kimm, T., Khaliq, Z.M., and Bean, B.P. (2015). Differential regulation of action potential shape and burst-frequency firing by BK and Kv2 channels in substantia nigra dopaminergic neurons. Journal of Neuroscience *35*, 16404–16417. https://doi.org/10.1523/JNEUROSCI.5291-14.2015.
46. Müller, A., Kukley, M., Uebachs, M., Beck, H., and Dietrich, D. (2007). Nanodomains of single Ca2+ channels contribute to action potential repolarization in cortical neurons. Journal of Neuroscience *27*, 483–495. https://doi.org/10.1523/JNEUROSCI.3816-06.2007.
47. Bock, T., and Stuart, G.J. (2016). The impact of BK channels on cellular excitability depends on their subcellular location. Front. Cell. Neurosci. *10*, 1–8. https://doi.org/10.3389/fncel.2016.00206.
48. Desai, N.S., Cudmore, R.H., Nelson, S.B., and Turrigiano, G.G. (2002). Critical periods for experience-dependent synaptic scaling in visual cortex. Nat. Neurosci. *5*, 783–789. https://doi.org/10.1038/nn878.
49. Wiesel, T.N., and Hubel, D.H. (1963). Single-cell responses in striate cortex of kittens deprived of vision in one eye. J. Neurophysiol. *26*, 1003–1017.
50. Wen, W., and Turrigiano, G.G. (2021). Developmental regulation of homeostatic plasticity in mouse primary visual cortex. The Journal of Neuroscience *41*, JN-RM-1200-21. https://doi.org/10.1523/jneurosci.1200-21.2021.
51. Trojanowski, N.F., and Turrigiano, G.G. (2021). CaMKIV signaling is not essential for the maintenance of intrinsic or synaptic properties in mouse visual cortex. eNeuro *8*, 1–12. https://doi.org/10.1523/ENEURO.0135-21.2021.
52. Griffen, T.C., Haley, M.S., Fontanini, A., and Maffei, A. (2017). Rapid plasticity of visually evoked responses in rat monocular visual cortex. PLoS One *12*, 1–12. https://doi.org/10.1371/journal.pone.0184618.
53. Gainey, M.A., Aman, J.W., and Feldman, D.E. (2018). Rapid disinhibition by adjustment of PV intrinsic excitability during whisker map plasticity in mouse S1. Journal of Neuroscience *38*, 4749–4761. https://doi.org/10.1523/JNEUROSCI.3628-17.2018.
54. Maravall, M., Stern, E.A., and Svoboda, K. (2004). Development of intrinsic properties and excitability of layer 2/3 pyramidal neurons during a critical period for sensory maps in rat barrel cortex. J. Neurophysiol. *92*, 144–156. https://doi.org/10.1152/jn.00598.2003.

55. Breton, J.D., and Stuart, G.J. (2009). Loss of sensory input increases the intrinsic excitability of layer 5 pyramidal neurons in rat barrel cortex. J. Physiol. *587*, 5107–5119. https://doi.org/10.1113/JPHYSIOL.2009.180943.
56. Sun, Q.Q. (2009). Experience-dependent intrinsic plasticity in interneurons of barrel cortex layer IV. J. Neurophysiol. *102*, 2955–2973. https://doi.org/10.1152/jn.00562.2009.
57. Li, L., Gainey, M.A., Goldbeck, J.E., and Feldman, D.E. (2014). Rapid homeostasis by disinhibition during whisker map plasticity. Proc. Natl. Acad. Sci. U. S. A. *111*, 1616–1621. https://doi.org/10.1073/pnas.1312455111.
58. Jamann, N., Dannehl, D., Lehmann, N., Wagener, R., Thielemann, C., Schultz, C., Staiger, J., Kole, M.H.P., and Engelhardt, M. (2021). Sensory input drives rapid homeostatic scaling of the axon initial segment in mouse barrel cortex. Nat. Commun. *12*, 1–14. https://doi.org/10.1038/s41467-020-20232-x.
59. Hickmott, P.W. (2005). Changes in intrinsic properties of pyramidal neurons in adult rat S1 during cortical reorganization. J. Neurophysiol. *94*, 501–511. https://doi.org/10.1152/jn.00924.2004.
60. Francis, H.W., and Manis, P.B. (2000). Effects of deafferentation on the electrophysiology of ventral cochlear nucleus neurons. Hear. Res. *149*, 91–105. https://doi.org/10.1016/S0378-5955(00)00165-9.
61. Lu, Y., Monsivais, P., Tempel, B.L., and Rubel, E.W. (2004). Activity-dependent regulation of the potassium channel subunits Kv1.1 and Kv3.1. Journal of Comparative Neurology *470*, 93–106. https://doi.org/10.1002/cne.11037.
62. Wang, Y., and Manis, P.B. (2006). Temporal coding by cochlear nucleus bushy cells in DBA/2J mice with early onset hearing loss. JARO - Journal of the Association for Research in Otolaryngology *7*, 412–424. https://doi.org/10.1007/s10162-006-0052-9.
63. Leao, R.N., Berntson, A., Forsythe, I.D., and Walmsley, B. (2004). Reduced low-voltage activated K+ conductances and enhanced central excitability in a congenitally deaf (dn/dn) mouse. J. Physiol. *559*, 25–33. https://doi.org/10.1113/JPHYSIOL.2004.067421.
64. Him, A., and Dutia, M.B. (2001). Intrinsic excitability changes in vestibular nucleus neurons after unilateral deafferentation. Brain Res. *908*, 58–66. https://doi.org/10.1016/S0006-8993(01)02600-2.
65. George, N.M., Gentile Polese, A., Merle, L., Macklin, W.B., and Restrepo, D. (2022). Excitable axonal domains adapt to sensory deprivation in the olfactory system. The Journal of Neuroscience *42*, 1491–1509. https://doi.org/10.1523/JNEUROSCI.0305-21.2021.
66. Barnes, B.Y.C.A., and McNaughton, B.L. (1980). Physiological compensation for loss of afferent synapses in rat hippocampal granule cells during senescence. J. Physiol *309*, 473–485. https://doi.org/10.1113/jphysiol.1980.sp013521ch.
67. Midorikawa, M., and Miyata, M. (2021). Distinct functional developments of surviving and eliminated presynaptic terminals. Proc. Natl. Acad. Sci. U. S. A. *118*. https://doi.org/10.1073/pnas.2022423118.
68. O'Leary, T., van Rossum, M.C.W., and Wyllie, D.J.A. (2010). Homeostasis of intrinsic excitability in hippocampal neurones: Dynamics and mechanism of the response to chronic depolarization. Journal of Physiology *588*, 157–170. https://doi.org/10.1113/jphysiol.2009.181024.
69. Pozzi, D., Lignani, G., Ferrea, E., Contestabile, A., Paonessa, F., D'Alessandro, R., Lippiello, P., Boido, D., Fassio, A., Meldolesi, J., et al. (2013). REST/NRSF-mediated intrinsic homeostasis protects neuronal

networks from hyperexcitability. EMBO Journal *32*, 2994–3007. https://doi.org/10.1038/emboj.2013.231.

70. Wefelmeyer, W., Cattaert, D., and Burrone, J. (2015). Activity-dependent mismatch between axo-axonic synapses and the axon initial segment controls neuronal output. Proc. Natl. Acad. Sci. U. S. A. *112*, 9757–9762. https://doi.org/10.1073/pnas.1502902112.
71. Malik, R., and Chattarji, S. (2012). Enhanced intrinsic excitability and EPSP-spike coupling accompany enriched environment-induced facilitation of LTP in hippocampal CA1 pyramidal neurons. J. Neurophysiol. *107*, 1366–1378. https://doi.org/10.1152/jn.01009.2011.
72. Valero-Aracama, M.J., Sauvage, M.M., and Yoshida, M. (2015). Environmental enrichment modulates intrinsic cellular excitability of hippocampal CA1 pyramidal cells in a housing duration and anatomical location-dependent manner. Behavioural Brain Research *292*, 209–218. https://doi.org/10.1016/j.bbr.2015.05.032.
73. Kole, M.H.P., Czéh, B., and Fuchs, E. (2004). Homeostatic maintenance in excitability of tree shrew hippocampal CA3 pyramidal neurons after chronic stress. Hippocampus *14*, 742–751. https://doi.org/10.1002/hipo.10212.
74. Kamal, A., Notenboom, R.G.E., De Graan, P.N.E., and Ramakers, G.M.J. (2006). Persistent changes in action potential broadening and the slow afterhyperpolarization in rat CA1 pyramidal cells after febrile seizures. European Journal of Neuroscience *23*, 2230–2234. https://doi.org/10.1111/j.1460-9568.2006.04732.x.
75. Eshra, A., Hirrlinger, P., and Hallermann, S. (2019). Enriched environment shortens the duration of action potentials in cerebellar granule cells. Front. Cell. Neurosci. *13*, 1–9. https://doi.org/10.3389/fncel.2019.00289.
76. Ngodup, T., Goetza, J.A., McGuire, B.C., Sun, W., Lauer, A.M., and Xu-Friedman, M.A. (2015). Activity-dependent, homeostatic regulation of neurotransmitter release from auditory nerve fibers. Proc. Natl. Acad. Sci. U. S. A. *112*, 6479–6484. https://doi.org/10.1073/PNAS.1420885112/-/DCSUPPLEMENTAL/PNAS.201420885SI.PDF.
77. Simkin, D., Hattori, S., Ybarra, N., Musia, T.F., Buss, E.W., Richter, H., Matthew Oh, M., Nicholson, D.A., and Disterhoft, J.F. (2015). Aging-related hyperexcitability in CA3 pyramidal neurons is mediated by enhanced A-type K+ channel function and expression. Journal of Neuroscience *35*, 13206–13218. https://doi.org/10.1523/JNEUROSCI.0193-15.2015.
78. Mehranfard, N., Gholamipour-Badie, H., Motamedi, F., Janahmadi, M., and Naderi, N. (2015). Long-term increases in BK potassium channel underlie increased action potential firing in dentate granule neurons following pilocarpine-induced status epilepticus in rats. Neurosci. Lett. *585*, 88–91. https://doi.org/10.1016/j.neulet.2014.11.041.
79. Raffaelli, G., Saviane, C., Mohajerani, M.H., Pedarzani, P., and Cherubini, E. (2004). BK potassium channels control transmitter release at CA3-CA3 synapses in the rat hippocampus. Journal of Physiology *557*, 147–157. https://doi.org/10.1113/jphysiol.2004.062661.
80. Moutin, E., Hemonnot, A.L., Seube, V., Linck, N., Rassendren, F., Perroy, J., and Compan, V. (2020). Procedures for culturing and genetically manipulating murine hippocampal postnatal neurons. Front. Synaptic Neurosci. *12*, 1–16. https://doi.org/10.3389/fnsyn.2020.00019.
81. Martiszus, B.J., Tsintsadze, T., Chang, W., and Smith, S.M. (2021). Enhanced excitability of cortical neurons in low-divalent solutions is primarily mediated by

altered voltage-dependence of voltage-gated sodium channels. Elife *10*, 1–26. https://doi.org/10.7554/eLife.67914.

82. Clements, J.D., and Bekkers, J.M. (1997). Detection of spontaneous synaptic events with an optimally scaled template. Biophys. J. *73*, 220–229. https://doi.org/10.1016/S0006-3495(97)78062-7.

83. Rothman, J.S., and Silver, R.A. (2018). Neuromatic: An integrated open-source software toolkit for acquisition, analysis and simulation of electrophysiological data. Front. Neuroinform. *12*, 1–21. https://doi.org/10.3389/fninf.2018.00014.

84. Debanne, D., Boudkkazi, S., Campanac, E., Cudmore, R.H., Giraud, P., Fronzaroli-Molinieres, L., Carlier, E., and Caillard, O. (2008). Paired-recordings from synaptically coupled cortical and hippocampal neurons in acute and cultured brain slices. Nat. Protoc. *3*, 1559–1568. https://doi.org/10.1038/nprot.2008.147.

85. Gong, Y., Huang, C., Li, J.Z., Grewe, B.F., Zhang, Y., Eismann, S., and Schnitzer, M.J. (2015). High-speed recording of neural spikes in awake mice and flies with a fluorescent voltage sensor. Science (1979). *350*, 1361–1366. https://doi.org/10.1126/science.aab0810.

86. Thevenaz, P., Ruttimann, U.E., and Unser, M. (1998). A pyramid approach to subpixel registration based on intensity. IEEE Transactions on Image Processing *7*, 27–41. https://doi.org/10.1109/83.650848.

87. Brown, L.D., Cai, T.T., and DasGupta, A. (2001). Interval estimation for a binomial proportion. Statistical Science *16*, 101–133.

1068 **Figures and legends**

1069

1070

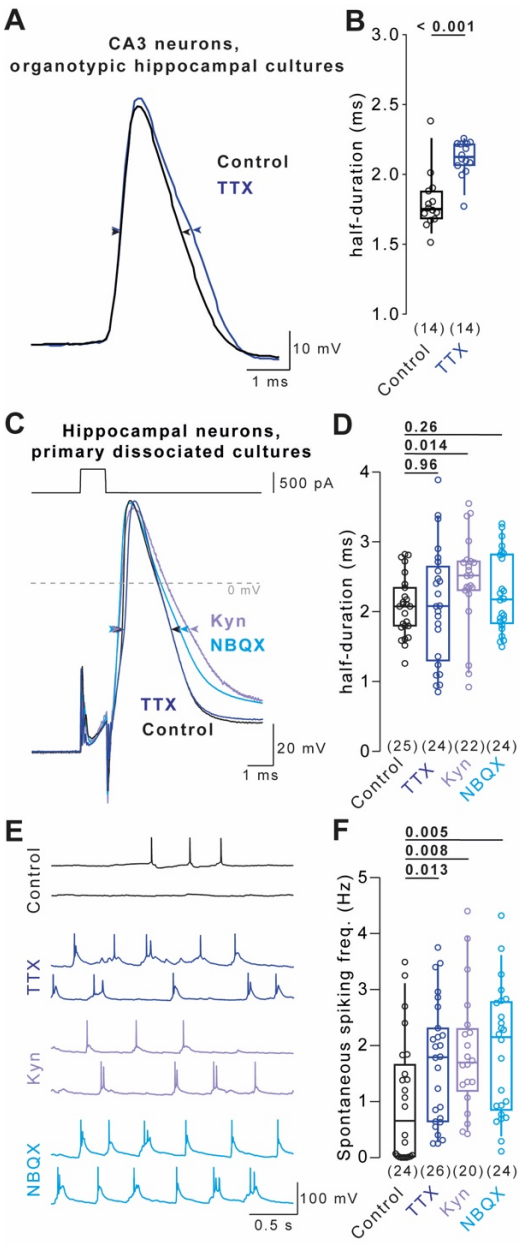

1071

1072

1073 **Figure 1 Cell type- and model-specific AP broadening in hippocampal neurons**

1074 (A) Example evoked APs recorded from CA3 pyramidal neurons in organotypic
1075 hippocampal cultures under control condition (black) and following 48 hours of
1076 TTX-treatment (blue).

1077 (B) AP durations recorded under conditions in A.

1078 (C) Example depolarization-evoked APs (500 pA for 1 ms) recorded from neurons in
1079 primary dissociated hippocampal cultures under control condition (black) and
1080 following 48 hours of TTX- (blue), Kyn- (purple), or NBQX-treatment (turquoise).

1081 (D) AP durations recorded under conditions in C.

1082 (E) Example spontaneous APs recorded under the conditions in C.

1083 (F) Spontaneous AP frequency under the conditions in C.

1084 Numbers in brackets reflect number of recorded neurons. Box plots as median ±
1085 interquartile range, whiskers indicate 10–90 percentile. P-values above graphs,
1086 significance tested by Mann-Whitney-*U* test.

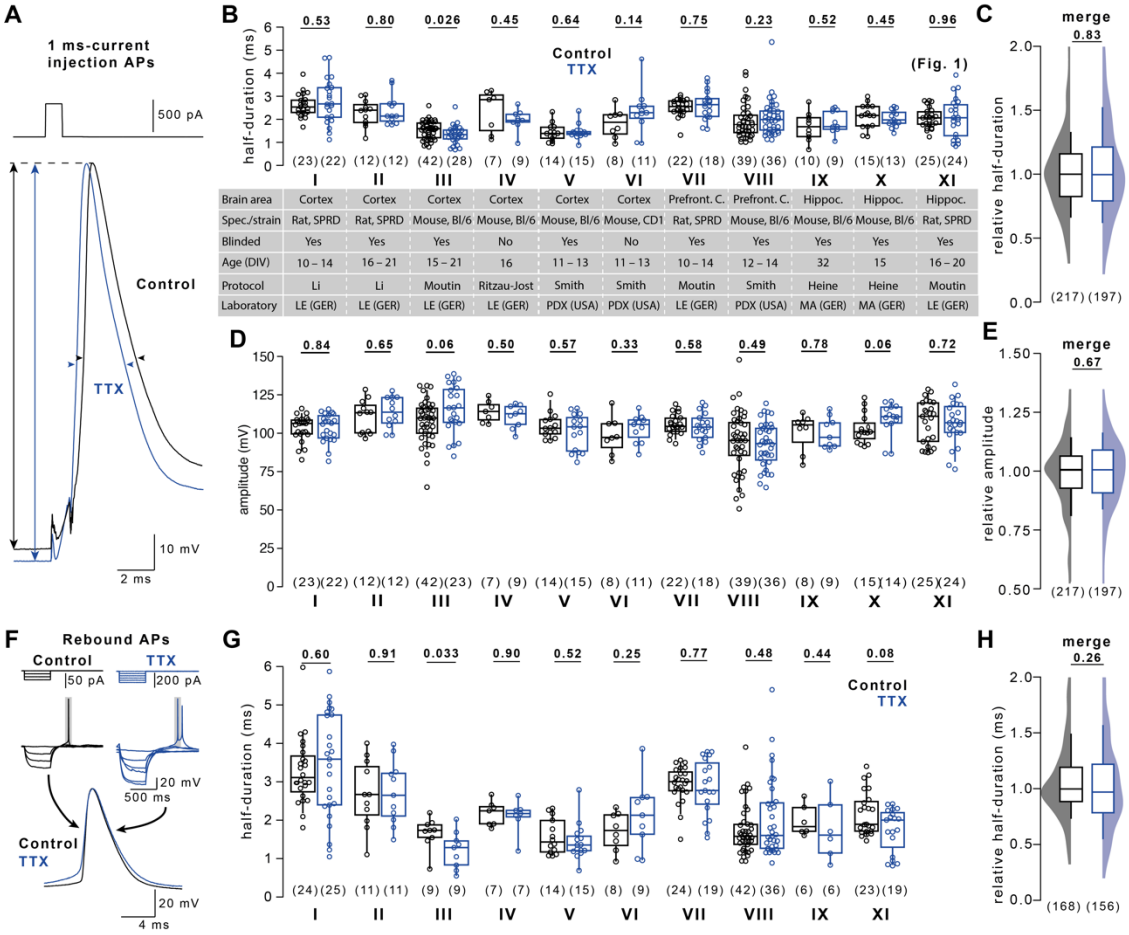

Figure 2 Stable AP duration in primary dissociated neurons during TTX-induced homeostatic plasticity

(A) Example current injection-evoked APs (500 pA for 1 ms) under control condition (black) and following 48 hours of TTX-treatment (blue). AP amplitudes are recorded between the membrane potential preceding the AP and AP peak (arrows), AP durations are recorded at half-maximal amplitude (arrow heads).

(B) AP duration in control and TTX-treated cells (color code as in A) for eleven different experimental conditions (I–XI). Specification of individual conditions is provided in Table S1. Condition XI adopted from Fig. 1D.

(C) Merge of AP durations in control and TTX-treated cells across conditions I–IX normalized to the corresponding condition's control median duration.

(D) AP amplitudes in control and TTX-treated cells as in B.

(E) Cross-conditional merge of AP amplitudes in control and TTX-treated cells as in C.

(F) Example hyperpolarization-evoked "rebound APs" (-150 pA or -60 pA for 500ms) in control and TTX-treated cells (color code as in A).

(G) Rebound AP duration in control and TTX-treated cells as in B.

1105 (H) Cross-conditional merge of normalized durations as in C for rebound APs.
1106 Numbers in brackets reflect number of recorded neurons. Box plots as median ±
1107 interquartile range, whiskers indicate 10–90 percentile. P-values provided above
1108 graphs; significance tested using Mann-Whitney-*U* tests.

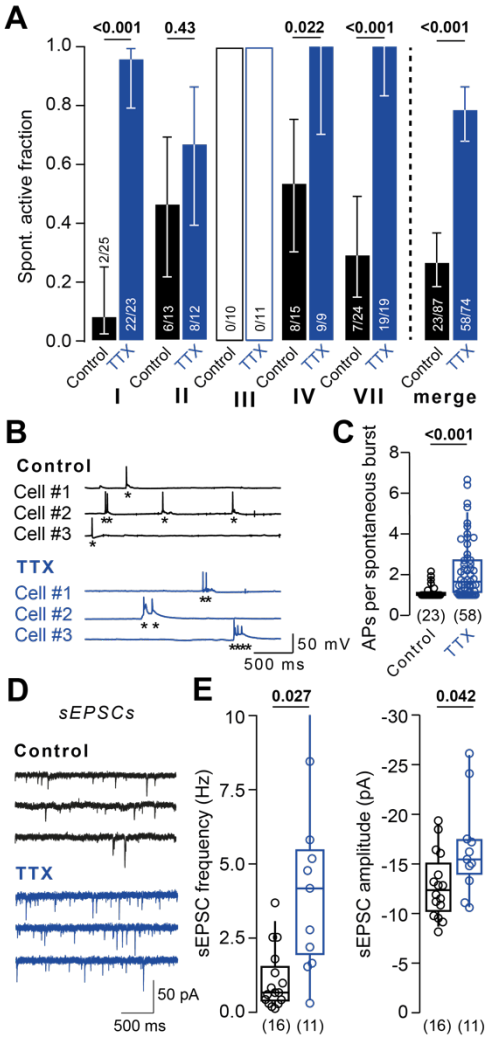

Figure 3 Homeostatic plasticity increases network activity and excitatory synaptic transmission

(A) *Left:* Spontaneously active control (black) and TTX-treated cells (blue) in condition I–IV and VII. *Right*: Active neurons merged across conditions I–IV and VII.

(B) Example spontaneous AP bursts in control and TTX-treated cells. Asterisks mark individual APs.

(C) AP number per burst in control and TTX-treated cells across conditions I–IV and VII.

(D) Example spontaneous excitatory postsynaptic currents (sEPSCs) in control and TTX-treated cells.

(E) *Left:* sEPSC frequency and *Right:* sEPSC amplitude in control recordings and after TTX-treatment (merged data from conditions I and II).

1124 Numbers in brackets reflect number of recorded neurons. Bars in A reflect fraction
1125 of spontaneously active neurons. Whiskers in A reflect confidence limits for 95%
1126 confidence interval based on Wilson interval. Box plots as median ± interquartile
1127 range, whiskers indicate 10–90 percentile. P-values above graphs, significance
1128 tested by Fisher's exact test in A or Mann-Whitney-*U* test elsewhere.

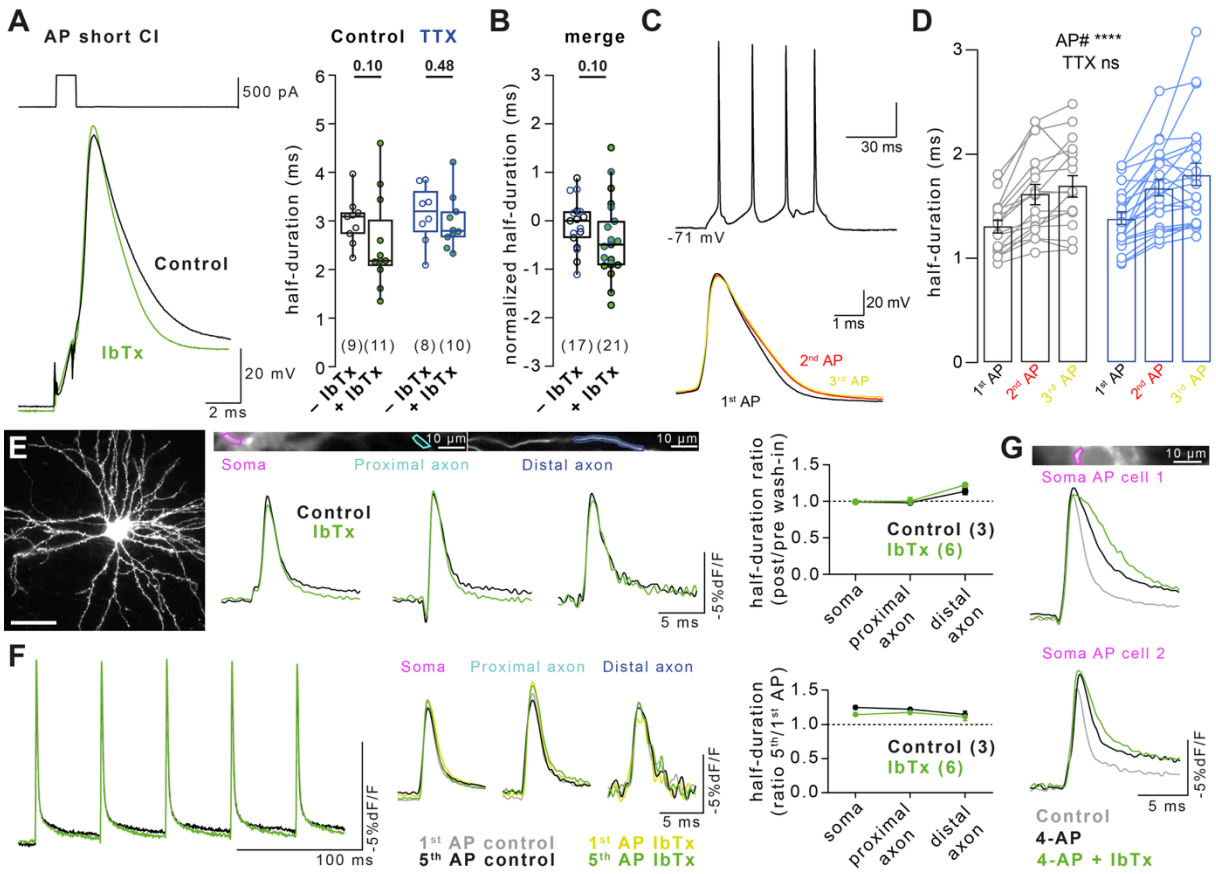

Figure 4 Lack of BK channel-dependent AP broadening in dissociated cultured neurons

(A) *Left:* Example current injection-evoked APs (500 pA for 1 ms) in control solution (black) and solution containing 300 nM Iberiotoxin (IbTx, green). *Right:* AP duration in control and TTX-treated cells recorded IbTx-free (black and blue, respectively) or IbTx-containing solution (green). Data recorded under condition I.

(B) Merged AP duration across control and TTX-treated cells for recordings in IbTx-free and IbTx-containing solution (data in A normalized to the respective group's median duration in control solution).

(C) APs evoked by a 200 ms current injection (top) and overlay of the forst three evoked APs (bottom).

(D) Broadening of AP duration of the 3 first APs during 200 ms current injections in control (black, *left*) and TTX-treated cells (blue, *right*). Bars as mean ± SEM, lines with markers depict recordings from individual neurons.

(E) *Left:* Example image of neuron expressing the genetically encoded voltage indicator Ace-mNeon (scale bar 50 µm). *Middle:* Example Ace-mNeon-recorded somatic, proximal axonal, and distal axonal APs in a primary hippocampal cultured neuron in IbTx-free solution (black) and following BK channel block by IbTx (100

1148 nM, green). *Right:* Ratio of somatic and axonal AP durations in IbTx-free and IbTx-
1149 containing solution.
1150 (F) *Left:* Example AP train (5 x 20 Hz) and overlay of 1st and 5th train AP at the soma,
1151 proximal, and distal axon in control condition (grey and black) and following BK
1152 channel block by IbTx (yellow and green). *Right:* AP broadening (ratio of 5th over
1153 1st train AP duration) in the three compartments in control and IbTx-containing
1154 solution.
1155 (G) Somatic APs under control condition (grey), following treatment with 4-AP (black),
1156 and following treatment with 30µM 4-AP + 100 nM IbTx (green).
1157 Numbers in brackets reflect number of recorded neurons. Box plots as median ±
1158 interquartile range, whiskers indicate 10–90 percentile. Plots in D–F as mean ± SEM.
1159 P-values above graphs, significance tested by Mann-Whitney-*U* test.

1160 **Figure supplements**

Group	Species	Strain	Brain area	Culture age (days *in vitro*)	Lab which recordings were performed at	External recor-ding solution	External [Ca^{2+}] (mM)	Internal recording solution	Growth medium	Protocol Reference
I	Rat	Sprague-Dawley	Cortex	10–14	Hallermann Lab, Leipzig (Germany)	1.)	2.0	5.)	NbActiv4	Li *et al.*, Cell 2020
II	Rat	Sprague-Dawley	Cortex	16–21	Hallermann Lab, Leipzig (Germany)	1.)	2.0	5.)	NbActiv4	Li *et al.*, Cell 2020
III	Mouse	C57BL/6N	Cortex	15–20	Hallermann Lab, Leipzig (Germany)	2.)	1.1	6.)	BrainPhys	Moutin *et al.*, Front. Synaptic Neurosci 2020
IV	Mouse	C57BL/6N	Cortex	16	Hallermann Lab, Leipzig (Germany)	2.)	1.1	6.)	MEM, 5% serum + supplements	Ritzau-Jost *et al.*, Cell Reports 2021
V	Mouse	C57BL/6J	Cortex	11–13	Smith Lab, Portland (OR, USA)	3.)	2.0	7.)	MEM, 5% serum + supplements	Martiszus BJ *et al.*, eLife 2021
VI	Mouse	CD1	Cortex	11–13	Smith Lab, Portland (OR, USA)	3.)	2.0	7.)	MEM, 5% serum + supplements	Martiszus BJ *et al.*, eLife 2021
VII	Rat	Sprague-Dawley	Pre-frontal cortex	10–14	Hallermann Lab, Leipzig (Germany)	1.)	2.0	5.)	BrainPhys	Moutin *et al.*, Front. Synaptic Neurosci 2020
VIII	Mouse	C57BL/6J	Pre-frontal cortex	10–14	Smith Lab, Portland (OR, USA)	1.)	2.0	8.)	MEM, 5% serum + supplements	Martiszus BJ *et al.*, eLife 2021
IX	Mouse	C57BL/6N	Hippo-campus	32	Heine Lab, Mainz (Germany)	4.)	2.0	9.)	Neurobasal A+ supplements	Li *et al.*, Cell 2020
X	Mouse	C57BL/6J	Hippo-campus	15	Heine Lab, Mainz (Germany)	4.)	2.0	9.)	Neurobasal A + supplements	Li *et al.*, Cell 2020
XI	Rat	Sprague-Dawley	Hippo-campus	16–20	Hallermann Lab, Leipzig (Germany)	1.)	2.0	5.)	BrainPhys	Moutin *et al.*, Front. Synaptic Neurosci 2020

1.) 122 NaCl, 3 KCl, 10 Glucose, 26 $NaHCO_3$, 2 $CaCl_2$, 1.3 $MgCl_2$, 1.25 NaH_2PO_4
2.) 125 NaCl, 3 KCl, 25 Glucose, 25 $NaHCO_3$, 1.1 $CaCl_2$, 1.1 $MgCl_2$, 1.25 Na_2HPO_4
3.) 150 NaCl, 4 KCl, 10 Glucose, 10 HEPES, 2 $CaCl_2$, 1 $MgCl_2$
4.) 145 NaCl, 2.5 KCl, 24 Glucose, 10 HEPES, 2 $CaCl_2$, 1.3 $MgCl_2$
5.) 130 K gluconate, 10 HEPES, 1 $MgCl_2$, 0.3 EGTA, 4 Mg-ATP, 0.3 Na-GTP, 10 Tris-Phosphocreatine
6.) 150 K gluconate, 10 K-HEPES, 10 NaCl, 0.05 EGTA, 3 Mg-ATP, 0.3 Na-GTP
7.) 135 K gluconate, 10 HEPES, 4 NaCl, 0.05 EGTA, 3 Na_2ATP, 0.3 NaGTP, 3 $MgCl_2$, 10 Na_2-Creatine phosphate
8.) 130 K gluconate, 10 HEPES, 0.3 EGTA, 4 Na_2ATP (or Mg-ATP), 0.3 NaGTP, 2 $MgCl_2$, 10 Na_2-Creatine phosphate (or Tris-Creatinine phosphate)
9.) 140 K gluconate, 20 HEPES, 2 NaCl, 0.5 EGTA, 4 Na_2ATP, 0.3 NaGTP, 3 $MgCl_2$

1161

1162

1163 **Figure 2 – figure supplement 1**

1164 **Additional information on recording conditions**

1165 The table lists additional relevant information on the experimental conditions I – XI.

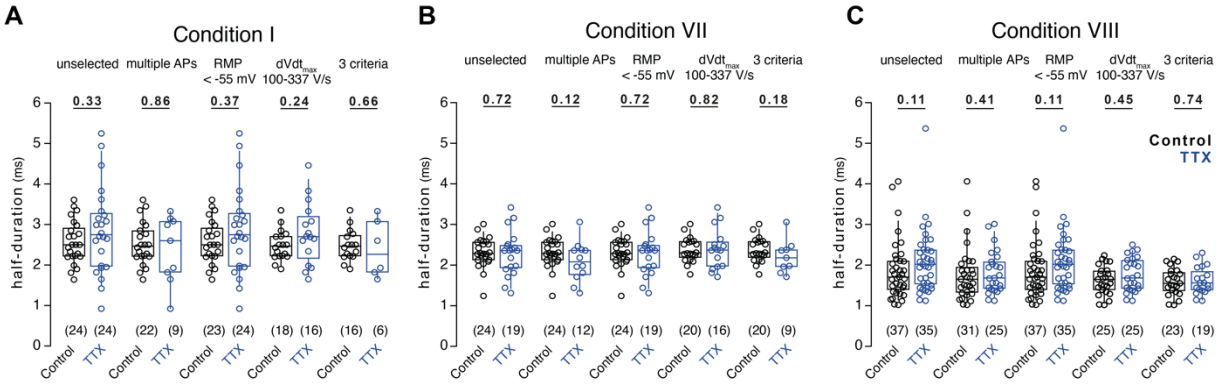

Figure 2 – figure supplement 2

Absence of TTX-induced AP broadening in further selected conditions

(A) Box plots of AP durations under control condition (black) or upon TTX-treatment (blue) recorded in condition I either unselected or selected for parameters reflecting unimpaired neuronal function.

(B) AP durations as in A for recordings in condition VII.

(C) AP durations as in A for recordings in condition VIII.

Numbers of recorded neurons provided in brackets. Box plots depict median ± interquartile range, whiskers reflect 10–90 percentile. P-values calculated by Mann-Whitney-*U* test.

1179

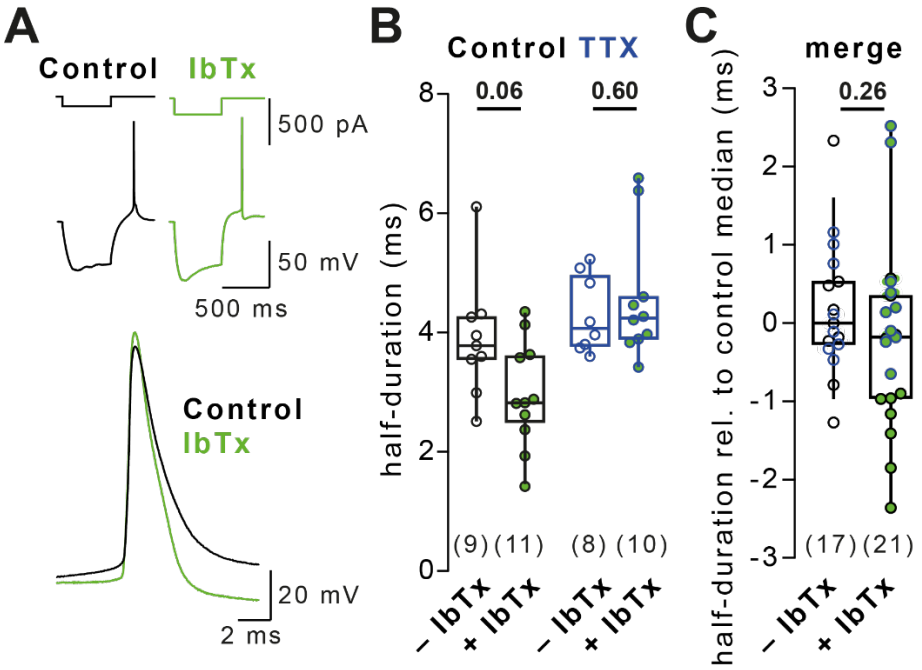

1180

1181

1182 **Figure 4 – figure supplement 1**

1183 **BK channel block does not affect rebound AP duration**

1184 (A) Example rebound APs in control solution (black) and solution containing 300 nM
1185 Iberiotoxin (IbTx, green).

1186 (B) AP duration in control and TTX-treated cells in IbTx-free (black and blue,
1187 respectively) or IbTx-containing solution (green). Data recorded in condition I.

1188 (C) Merged AP duration across control and TTX-treated cells for recordings in IbTx-
1189 free and IbTx-containing solution (data in A, normalized to the respective group's
1190 median duration in IbTx-free solution).

1191 Numbers of recorded neurons provided in brackets. Box plots depict median ±
1192 interquartile range, whiskers reflect 10–90 percentile. P-values calculated by Mann-
1193 Whitney-*U* test.